Received: 16 June 2015 | Accepted: 26 August 2016

DOI 10.1002/hyp.11030

WILEY

RESEARCH ARTICLE

Groundwater—Surface waters interactions at slope and catchment scales: implications for landsliding in clay-rich slopes

Vincent Marc[1] | Catherine Bertrand[2] | Jean-Philippe Malet[3] | Nicolas Carry[2] | Roland Simler[1] | Federico Cervi[1,4]

[1] EMMAH—Environnement Méditerranéen et Modélisation des Agro-Hydrosystèmes, INRA UMR 1114, Université d'Avignon et des Pays de Vaucluse, 33 rue Louis Pasteur, Avignon F-84000, France

[2] Chrono-Environnement CNRS UMR 6249, Université de Franche-Comté, 16 Route de Gray, Besançon F-25030, France

[3] Institut de Physique du Globe de Strasbourg, CNRS UMR 7516, Université de Strasbourg/EOST, 5 rue René Descartes, Strasbourg F-67084, France

[4] University of Bologna, Department of Civil, Chemical, Environmental and Materials Engineering (DICAM), Viale Risorgimento 2, Bologna 40136, Italy

Correspondence
Vincent Marc, EMMAH—Environnement Méditerranéen et Modélisation des Agro-Hydrosystèmes, INRA UMR 1114, Université d'Avignon et des Pays de Vaucluse 33 rue Louis Pasteur, Avignon F-84000, France.
Email: vincent.marc@univ-avignon.fr

Abstract

Understanding water infiltration and transfer in soft-clay shales slopes is an important scientific issue, especially for landsliding. Geochemical investigations are carried out at the Super-Sauze and Draix-Laval landslides, both developed in the Callovo-Oxfordian black marls, with the objective to define the origin of the groundwater. *In situ* investigations, soil leaching experiments and geochemical modeling are combined to identify the boundaries of the hydrological systems. At Super-Sauze, the observations indicate that an external water flow occurs in the upper part of the landslide at the contact between the weathered black marls and the overlying formations, or at the landslide basement through a fault network. Such external origin of water is not observed at the local scale of the Draix-Laval landslide but is detected at the catchment scale with the influence of deep waters in the streamwater quality of low river flows. Hydrogeological conceptual models are proposed emphasizing the role of the interactions between local (slope) and regional (catchment) flow systems. The observations suggest that this situation is a common case in the Alpine area. Expected consequences of the regional flows on slope stability are discussed in term of rise of pore water pressures and physicochemical weathering of the clay shales.

KEYWORDS

black marls, Draix-Laval, geochemical modelling, hydrology, landslide, Super-Sauze

1 | INTRODUCTION

Landslide triggering is mostly related to hydrological factors governing infiltration and hydraulic head variations (Iverson and Major, 1986; Iverson, 2000; Montgomery and Dietrich, 1994; Ng and Shi, 1998; Van Asch et al., 1999; Cappa et al., 2004). Hydrological triggering is due to (a) an increase in pore water pressure, which results in the decrease of shear strength or (b) the generation of fully saturation conditions producing the overlap of the yield stress and the initiation of flow-like phenomena (Malet et al., 2003). In this context, the question of the behavior of the vadose and saturated zones and the origin of water is crucial for understanding and forecasting slope instability.

Answering this question is usually addressed with several assumptions, such as (a) the representation of the processes at the hillslope scale and at a daily to monthly scales, (b) the simulation of vertical water infiltration and lateral transfer within thin soil layers, and (c) the simplification of the geometry of the local slope aquifers with constant hydrological properties and an impervious bedrock with a dip parallel to the slope surface. Moreover, local rainfall and snowmelt are generally considered as the only water sources for the recharge of shallow groundwater systems. But the large scale tectonic stresses, which have characterized the development of the mountain chain, may deeply impact the groundwater circulation (Tóth, 1999; Goldscheider and Neukum, 2010). The hydrological role of discontinuities have been proven in both lithified and unlithified siliciclastic materials as well as in crystalline and volcanic rocks (Forster and Evans, 1991; Seaton and Burbey, 2005; Bense et al., 2013). In particular, by allowing the development of preferential flow-paths driving groundwater from far away, they can lead to the creation of multi-scale hydrological systems (Tóth, 1999) in which spatial connections among different reservoirs are possible (Roques et al., 2014). The role of these geological structures and of the possible preferential water flows has already been demonstrated for controlling slope instability (Guglielmi et al., 2000; Bonzanigo et al., 2001; Cervi et al., 2012; Vallet et al., 2015). However, at the best of our knowledge, no work concerned the analysis of the interaction between local (1–10 km) and meso-scale (10–100 km)

hydrological systems, limiting the representativeness of simplified hydrological models as they mislead the water origin and flow paths.

The groundwater chemical composition represents a signature of the hydrological processes taking place beneath the soil surface; thus, water sampling is commonly considered a powerful tool for gathering hydrochemical information and unravels the abovementioned points (Calmels et al., 2011 ; Kim et al., 2014). Furthermore, many authors have reported that water chemistry and physicochemical processes have an impact on the soil stresses and slope stability (Di Maio et al., 2004, 2014; Picarelli et al., 2006).

Recently, geochemical modelling was used to explain observed changes of the groundwater chemistry (Motellier et al., 2003; Gaucher et al., 2006; de Montety et al., 2007). In most cases, the approach consisted in simulating the dissolution and precipitation of mineralogical phases until equilibrium between the media and the water was reached (thermodynamic-based approach). However, in highly dynamic hydrological systems such as shallow deforming groundwater systems (e.g., landslides), the thermodynamic equilibrium is not reached, and a kinetics-based approach is required to fully constrain the chemical and mixing processes. This was, for instance, the main limitation of the geochemical-based conceptualization of the hydrological system of the Super-Sauze landslide proposed by de Montety et al. (2007). Another limitation of this work was the use of a seasonal sampling procedure. Therefore, the present work uses a new hydrochemical database consisting in monthly water samples (from June 2010 to May 2011) and original isotopic data.

The work analyzed the datasets acquired on two slow-moving landslides (Super-Sauze and Laval-Draix, South French Alps) affecting black marls. Water flow processes have been previously investigated using different approaches. In particular, a first hydrological modelling exercise has been proposed at Super-Sauze by Malet et al. (2005) with a conceptual 3-D description of rapid infiltration. Despite the use of a complex hydrological model integrating a layered geometry and the use of different hydrological parameters, the authors had difficulties at understanding the water flow-paths within the landslide body, with a final consistent mismatch between the observed values and the model outputs. On the same site, similar problems have been found by Krzeminska et al. (2013) using a more complex model integrating exchange of water in the subsurface between a system of fissures and the matrix. Such difficulties were experienced on other large and complex landslides systems (Brunsden, 1999; Tacher et al., 2005).

The objective of this work is to integrate information from hydrochemistry, isotopic data, laboratory leaching experiments, and numerical simulations to (a) investigate the relevance of combined experimental approaches and geochemical modelling for the identification of the water origin and the hydrological systems boundaries and (b) discuss the possible role of the interactions between local and regional water systems on the landslide dynamics.

2 | GEOLOGICAL AND HYDROGEOLOGICAL SETTINGS

The two landslides investigated have developed in the Callovo-Oxfordian black marls of South East France (Maquaire et al., 2003): the Draix-Laval shallow landslide is located in the Draix-Bléone catchment and the Super-Sauze deep-seated landslide is located in the Ubaye catchment (Barcelonnette Basin; Figure 1). A detailed geomorphological description of the landslides is available in earlier works (Flageollet et al., 1999a; Fressard, 2008). In this manuscript, the regional geological context is presented in order to portray the multi-scale hydrological systems and their possible impacts on local landsliding.

2.1 | Regional geological context

The main geological structure observed in the region is the Digne thrust sheet (set up between Miocene and Pliocene) which is over thrusting autochthonous tertiary formations of the Digne-Valensole basin (Figure 1; Haccard et al. 1989). The main part of the thrust sheet is affected by N140°oriented folds associated with dextral strike-slip faults. This is the situation observed at the Draix-Laval site.

At the North-East, the Digne thrust sheet is topped with the Ubaye-Embrunais thrust sheets where the Super-Sauze landslide is located. These thrust sheets comprise the upper Parpaillon sheet lying through an unconformable contact over the autochthonous Callovo-Oxfordian black marls (Kerckhove et al., 1974) also named "Terre Noires." Locally, klippes scoured by erosion of the Parpaillon sheet thrust are observed.

2.2 | Geology and hydrology at the Super-Sauze slope

The Super-Sauze landslide is entirely developed in the "Terres Noires." It is located 300 m below the klippe of Lan (Figure 2a). This klippe is made of mid Trias to Eocene series in which a succession of dolomite, gypsum with enclosures of crushed dolomite and argillites, is observed (Pairis, 1968). The setting of the Parpaillon sheet thrust is dated from Miocene, but the autochthonous basement, mainly represented by the Callovo-Oxfordian black marls, has experienced intense tectonics processes. During upper Miocene, the rise of the external crystalline massifs resulted in the creation of long meridian faults changing the flexures in the "Terres Noires."

The "Terres Noires" are characterized by a thickness of 250–300 m of black clay-shales, very finely laminated (Maquaire et al., 2003). The tectonic contacts are often covered by 3–15-m-thick till deposited by the Ubaye glacier during the Quaternary age.

The Super-Sauze landslide has been triggered in the 1960s on the upper part of the Sauze torrent. It extends over a horizontal distance of 850 m between the elevation of 2,105 m (crown) and 1,740 m (toe) with an average 25° slope (de Montety et al., 2007). A network of 20 open standpipe piezometers is present since 1996, and it allows the water level monitoring and groundwater sampling at different depths.

The slope is characterized by a dry and mountainous Mediterranean climate with a significant interannual rainfall variability (733 ± 400 mm over the period 1928–2002; Malet, 2003), large rain storm intensity (>50 $mm{\cdot}h^{-1}$; Flageollet et al., 1999b,) and a large contribution of snowfall in the yearly precipitation amounts (up to 35%; Sommen, 1995, cited in Malet, 2003).

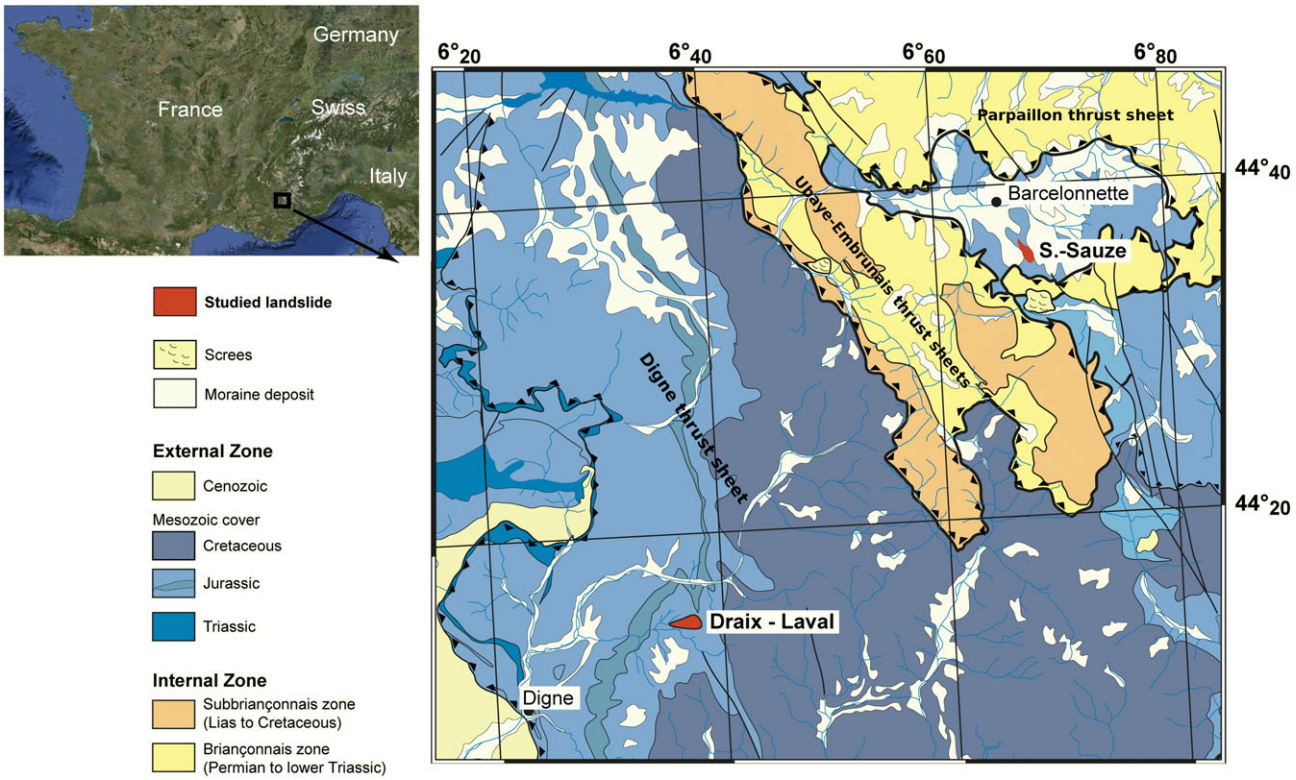

FIGURE 1 Regional geological context of the Super-Sauze and Draix-Laval landslides

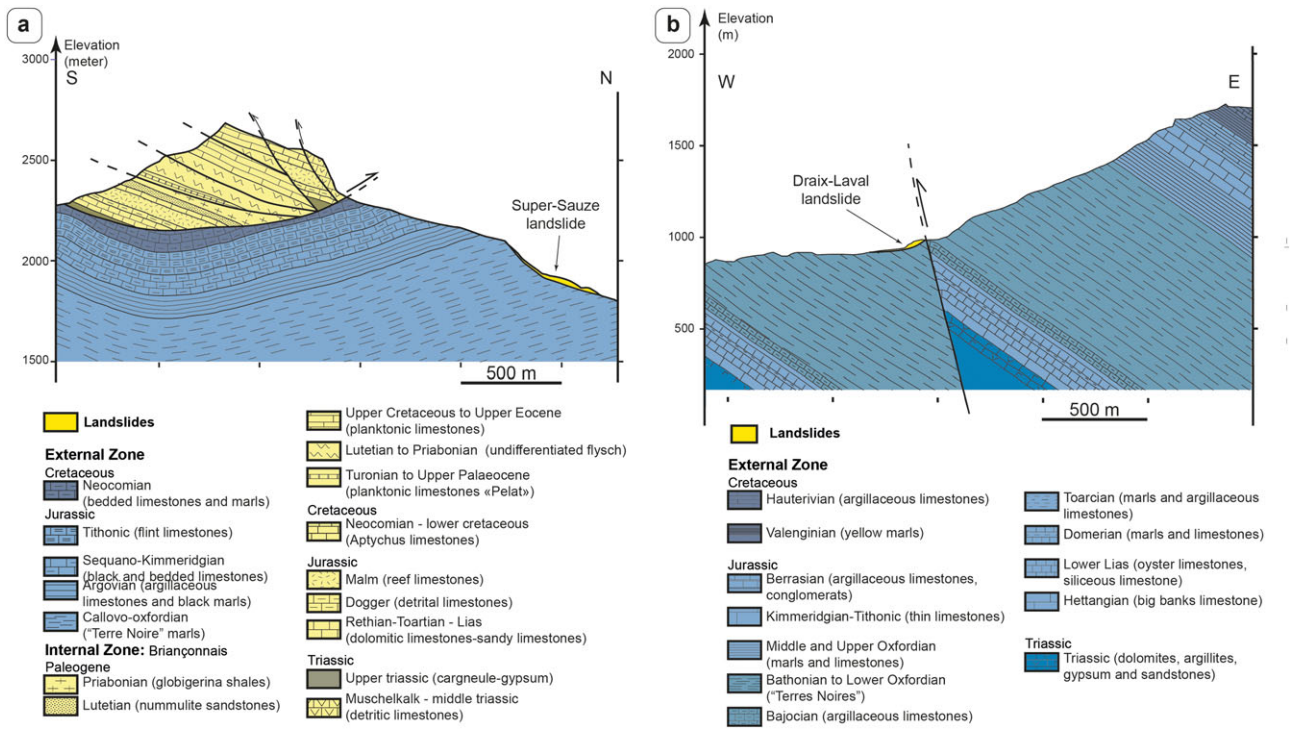

FIGURE 2 Geological cross sections of the Super-Sauze landslide (a) and the Draix-Laval catchment (b)

The hydrologeological context has been investigated since 1997 and was described in detail in by Malet et al. (2005) and de Montety et al. (2007). The main feature is the presence of an unconfined, shallow and continuous hydrogeological system (1- to 2.5-m depth) with water level changes according to the season and the recharge conditions. The main recharge period is springtime because of snow melting, while a second minor infiltration phase occurs in autumn. After the last recharge time, the usual behavior is a gradual and slow drainage until April–May of the next year.

2.3 | Geology and hydrology at the Draix-Laval slope

In the Digne region, the autochthonous black marls are less deformed than in the Ubaye region and present a small dip mostly caused by post-thrust deformation (Figure 2b). The region is crossed by the Col de la Cine dextral strike-slip fault dated from Oligocene (de Graciansky, 1972). This tectonic feature also acts as a thrust. The Dogger, the Lias, and locally, the Trias formations overlap the Bathonian, Callovian, and early Oxfordian ("Terres Noires").

The monitoring systems in the Draix-Bléone catchments, installed in the beginning of the 1980s, consist of several subbasins (for access to the observations, see https://bdoh.irstea.fr/DRAIX/). The Laval basin is the largest catchment with a total extension of 86 ha and a maximum elevation of 1,259 m a.s.l. The gauge section is situated at 847 m a.s.l., and the mean slope is 30°. The "Terres Noires" widely outcrop in the catchment, with a maximum thickness of 1,500 m. A shallow slide (e.g., Draix-Laval landslide) occurred in December 1998 in the middle of the catchment. The total extent is 180 m, and the elevations range between 880 and 930 m. The mean slope is 55°, and the surface is 0.4 ha. It evolves downslope into reworked marls and blocks. It has been instrumented with a network of five open standpipe piezometers (mean depth of 3 m) since 2006 (Garel et al., 2012; Travelletti et al., 2012).

The mean annual rainfall is 912 mm ± 188 m (over the period 1984–2008, Garel, 2010) with approximately 200 days without rainfalls and only 5 days with rainfall higher than 30 mm. Maximum precipitation and runoff occur in spring (April–May) and autumn (September–October), while summers are generally warm and with rainfall associated with short intensive thunderstorms (more than 60 $mm{\cdot}h^{-1}$; Borgès, 1993).

The hydrological context of the Draix-Laval landslide was described in Garel (2010), Travelletti et al. (2012), and Garel et al. (2012). They observed a shallow unconfined aquifer that is highly reactive to rainfall pulses. Infiltration processes were also investigated from a large-scale controlled rainfall experiment (Travelletti et al., 2012). Results from soil moisture, groundwater level monitoring, and tracing demonstrated the high infiltrating capacity of the material and the important role of the structure and of the macropore connectivity.

3 | METHODS

A multi-technique investigation strategy combining hydrogeochemical (groundwater electrical conductivity monitoring, groundwater isotopic, and chemical analysis, leaching experiments) and mineralogical (soil composition assessment) surveys has been carried out on both sites.

Groundwater chemistry and stable isotope analyses were used to characterize water/rock interactions. Leaching experiments have been carried out on soil samples from several black marls outcrops in order to control if water chemistry matches the mineralogical composition of the soil and rock. The geochemical model PHREEQC (Parkhurst and Appelo, 2013) was used in order to simulate the chemical interaction between different water composition and the soil and rocks. Models setups have been calibrated by carrying out further simulations on leaching tests. The methodological approach is summarized in Figure 3.

3.1 | Analysis of water chemistry: Field and laboratory measurements

Water measurements and sampling were carried out from June 2010 to May 2011 at both sites. The access to the Super-Sauze site was not possible in winter (from December to March) because of the presence of a thick snow cover. Outside this period, water sampling was carried out monthly. The sampling network consisted in six open standpipe piezometers (four at Super-Sauze and two at Draix-Laval) installed at depths of 3 m. At Super-Sauze, the four piezometers are considered representative of the complex hydrological behavior of the landslide, as proposed by Malet et al. (2005) and Krzeminska et al. (2013): A6 (upper part, A transect), BD (B transect), CP (C transect), and DV (close to the toe, D transect; Figure 4a). At Draix, the two piezometers (GC3 and GC4) are located in the lower part of the slope where a permanent groundwater table is observed (Figure 4b). Three sections were also monitored in the Laval stream (noted L in Figure 4b). In all piezometers, the samples were collected using a low-flow pump (0.1 $l{\cdot}s^{-1}$) after removing the old standing water.

Direct measurements of water temperature, acid potential pH, and specific conductance SC at 25°C were determined in the field using a (WTW, Weilheim, Germany) pH/cond 340i SET instrument equipped with a Ross glass electrode. The instrument was calibrated in the laboratory before each sampling campaign. Total alkalinity (TA) was measured at the laboratory by acidimetric titration with 0.02 N H_2SO_4 according to the Gran method (Gran, 1952) less than 48 hr after sampling. All water samples were filtered through cellulose membranes (0.45 μm) and stored in polyethylene bottles. Aliquots for cation analysis were acidified with HNO_3 at 69%. Water for isotope analysis (^{18}O and ^{2}H) was collected in 20-ml tinted glass bottles.

3.2 | Soil sampling and leaching experiments

Three soil samples (500 g each) were collected at the Super-Sauze landslide in the vicinity of the piezometers BD, CP, and DV. Two samples (RDC and RGC) were taken at the Draix–Laval landslide, close to piezometers GC3 and GC4, respectively. All samples were collected at 0.20-m depth (Figures 4a, b) and used for the leaching experiments. According to the USGS Field Leach Test (2005), 50 g of dried material was sieved at less than 2 mm, leached into 1 L of deionised water and continuously stirred by a magnetic agitator (with constant rotation speed of 200 rpm). The experiments lasted over a maximum of 10 hr, so that evaporation inside the container could be ignored.

3.3 | Geochemical analyses

The anions (Cl, NO_3, and SO_4) and cations (Na, K, Ca, and Mg) distribution was analyzed using ion chromatography (Dionex, Waltham, MA USA DX-120). Repeatability of the samples is <0.5%, and measurement uncertainty is comprised between 3% and 5%, depending on the concentration of the sample. Data on $\delta^{18}O(H_2O)$ were obtained according to the CO_2 gas equilibration technique, which relies on isotopic exchange of the oxygen atoms in the water and in the CO_2 (Epstein and Mayeda, 1953). Deuterium content was measured using the Cr reduction method. Analyses were performed with a VG (ISOPRIME,

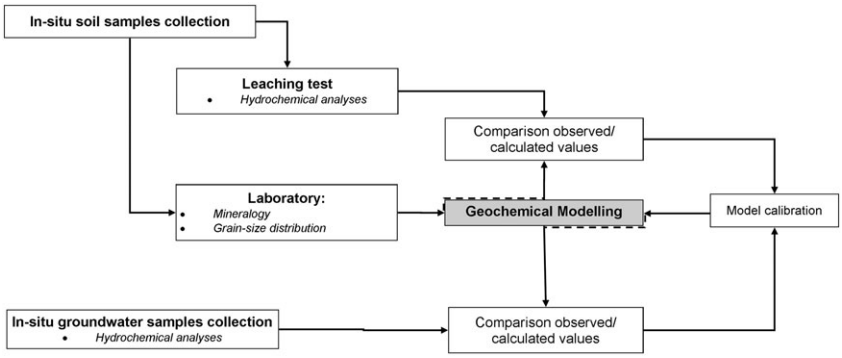

FIGURE 3 Flow chart of the methodological approach

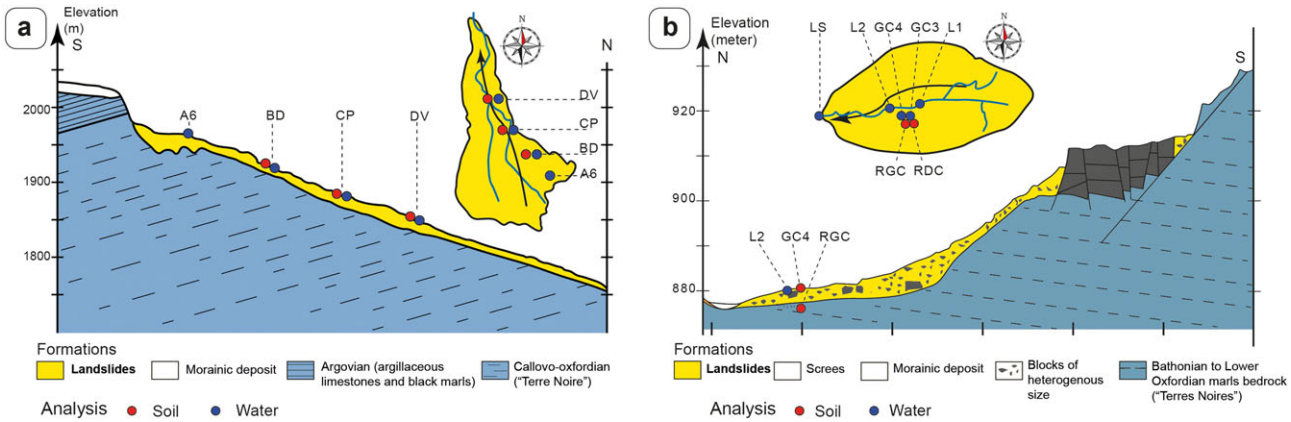

FIGURE 4 Location of the water samples (blue dots) and the soils samples (for leaching experiments, red dots) at Super-Sauze (a) and Draix-Laval (b)

Stockport, UK) mass spectrometer in continuous flow with (Aquaprep, Stockport, UK) and pyrolyser (EUROVECTOR, Stockport, UK) PyrOH. The sample values are expressed with reference to the Vienna-Standard Mean Ocean Water standard according to Equation 1:

$$\delta = \frac{R_{sample} - R_{std}}{R_{std}} \times 1000, \quad (1)$$

where R is the isotope ratio.

The uncertainty of mass spectrometric measurements is ±0.2‰ (with a 90% confidence level) for the 67 samples.

3.4 | Mineralogical analyses

The mineralogy of the soil samples used for the leaching tests has been investigated using X–ray diffractometry on oriented paste of the <2-µm fraction. The results are summarized in Table 1. Soil samples were analyzed at the Centre de Recherche et d'Enseignement de Géosciences de l'Environnement X-Ray service using a Panalytical X'Pert Pro MPD θ–θ diffractometer equipped with a back monochromator, a fast detector X'celerator, and working with an anticathode of cobalt. The calcite proportion was estimated by acidification with HCl 5% and a weighing of the samples before and after acidification. The relative proportions of quartz-calcite and of calcite-dolomite were obtained using the area of the mean peaks and comparison of the surfaces ratio with charts. The actual amounts of quartz-calcite and calcite-dolomite were calculated from their relative proportions and the absolute quantity of calcite measured with acid etching. For the clays, the percentage of minerals was calculated according to the ratio of the main peaks areas.

At the Super-Sauze landslide, the mineralogy of the black marls was determined from 15 soil samples collected at five locations according to different positions on the slopes and at three depths (de Montety et al., 2007). At the Draix-Laval landslide, 12 soil samples were taken at five locations at three depths (Garel, 2010). The maximum depth was 3 m, and the material samples were averaged over 1-m cores. Mean and standard deviation values are presented in Table 1. At Super-Sauze, the proportion of different minerals is relatively constant, which reflects a good homogeneity of the material. The main mineral phase is illite with an average of about 40% and quartz and carbonates with the same proportion of about 20%. There is a small percentage of chlorite, albite, and interstratified illite/smectite. At Draix-Laval, the samples differ by the presence of interstratified illite/smectite and by the presence of kaolinite. These results are in agreement with the previous data obtained by Maquaire et al. (2003) and de Montety et al. (2007).

Pyrite is known to exist in these rocks as vein-shaped material, so that a large variability in content is observed. In particular, the subaerial conditions of the soil samples make difficult the estimation of pyrite because the oxidation processes can alter this phase quickly. Pyrite is contained only within the "pure" black marl and is

TABLE 1 Mean mineralogical features of the Super-Sauze and Draix-Laval marls (g per 100 g of rock)

	Quartz	Calcite	Dolomite	Albite	Smectite	Illite	Smectite/Illite	Chlorite	Kaolinite
Super-Sauze									
Mean	20.5	21.3	7.1	1.6	0.3	39.2	4.8	3.3	
Standard deviation	3.8	2.4	0.8	0.2	0.7	2.6	1.5	1.3	
Draix-Laval									
Mean	17.7	23.7	4.7	1.0		11.7	30.9	5.5	4.9
Standard deviation	2.1	2.5	0.6	0.0		0.6	3.8	0.3	1.6

the only source of S, which in turn oxidizes and leads to secondary minerals. This pyrite can be in the bedrock or unweathered blocks within the landslides, while secondary minerals are widespread within the unsaturated zone.

3.5 | Geochemical modelling

3.5.1 | Modelling strategy

The chemical composition of water resulting from water–rock interaction is due to complex processes that can be described in terms of (a) mass transfers through the rock matrix and fractures, (b) reversible ions exchange reactions or irreversible minerals dissolution, and (c) precipitation of new mineralogical phases. In the case of non weathered Callovo-Oxfordian shales, several studies used geochemical modelling to estimate pore water chemical composition (Motellier et al., 2003; Gaucher et al., 2006; De Combarieu et al., 2007; Appelo et al., 2008; Beaucaire et al., 2008; Tournassat et al., 2008). Pearson et al. (2011) reviewed the assumptions used in geochemical modelling in such contexts. In most cases, thermodynamic equilibrium is assumed and ions exchange reactions are the main processes that explain pore water chemistry. These assumptions are relevant taking into account the very low hydraulic conductivity measured in the non weathered medium (10^{-15} to 10^{-12} m·s^{-1}; Delay et al., 2006) resulting in low velocities in reducing conditions. Ion exchange reactions are quick processes, and adsorbed cations are immediately in equilibrium with the pore water. The thermodynamic equilibrium is also reached for all the mineral phases, in particular, the calcite-dolomite-kaolinite-quartz system, while the stability of pyrite is ensured by the reducing condition in the medium.

In our case, the hydraulic conductivity values of the weathered material ranging from 10^{-7} to 10^{-5} ms^{-1} (Malet et al., 2005; Esteves et al., 2005; de Montety et al., 2007) suggest that the water turnover is fast and the thermodynamic equilibrium is not reached. At Super-Sauze and Draix-Laval, the investigated groundwaters are located in the marly regolith in close contact with the atmosphere. In such oxidizing conditions, the increase of sulfate concentration according to the main flow line is mainly explained by pyrite dissolution (de Montéty et al., 2007). This irreversible reaction produces protons, which generate carbonate dissolution. This behavior points out that reversible ions exchange is a marginal mechanism in our systems. Another point is the nature of the clays. In the Super-Sauze and Draix-Laval shales, the part of inter-stratified illite/smectite is very low compared with the proportion measured in other clay-shale environment (e.g., Bure and Mont Terri sites; Motellier et al., 2003; Pearson et al., 2011) where these dominant phases prove to have the highest cation exchange capacity. For these reasons, the modelling strategy in this study is focused on irreversible reactions. Unlike de Montety et al. (2007), we also took into account the kinetics of the minerals dissolution.

For a quantitative analysis, the modelling approach requires a good knowledge of the reactive surface for all the mineral phases. The actual reactive surfaces are very complex to estimate and most authors admit that their values are far lower than those estimated from a spherical or rough geometry (Gaus et al., 2005; Lüttge, 2005). This situation is expected for all minerals, but its impact on the dissolution is limited if the mineral solubility is low. As the mineral grain size was estimated from the literature (see section 3.5.2), our results must be considered as semi-quantitative. The adopted strategy was to estimate initial values of the reactive surfaces from the grain geometry and further optimize them to fit with the observed concentrations. This approach aims at comparing the modeled and observed concentrations over a reasonable range of reactive surfaces. The optimized values of reactive surfaces are discussed.

3.5.2 | Modeling parameters

Geochemical modeling was performed at the laboratory and field scales. At the laboratory scale, the model used the results from the soil leaching experiments. It aimed at explaining the processes of soil-water interactions and determining the calibration parameters for the simulation of the *in situ* processes.

The reaction path model between meteoric water (in the case of field-scale) and deionised water (in the case of leaching simulations) and the black marls material was simulated with PHREEQC 3 code (Parkhurst and Appelo, 2013) coupled to the LLNL database (Lawrence Livermore National Laboratory thermodynamic database, *llnl.dat*). PHREEQC simulates the soil alteration by the dissolution of the primary minerals and the precipitation of new phases; for each step, it calculates the quantity of destroyed or formed phases per kilogram of water, according to the mineral assemblage and the kinetic parameters of each phase (e.g., the thermodynamic data, kinetics constants, and reactive surfaces).

Kinetic laws are considered for all environments (acid, neutral, and basic) using Equation 2:

$$V_d = k_d \cdot S \cdot (a_{H^+})^n \cdot \left[1 - \exp\left(\frac{A}{R \cdot T}\right)\right] \Leftrightarrow V_d = k_d \cdot S \cdot (a_{H^+})^n \cdot \left[1 - \frac{Q}{K}\right]. \quad (2)$$

Williamson and Rimstidt (1994) proposed an expression for the oxidation rate of pyrite characterized by a square root dependence

on the molality of oxygen and a small increase of the rate with an increase in pH. This rate is applicable for the dissolution reaction only and only when the solution contains oxygen, according to Equation 3.

$$V_d\ pyrite = k_d \cdot S \cdot aO_2^{0.5} \cdot (a_{H^+})^{-0.11} \cdot \left[1 - \frac{Q}{K}\right], \quad (3)$$

where V_d is the dissolution rate (mol·s^{-1}), k_d is an empirical constant (mol·cm^{-2}·s^{-1}), A is the Arrhenius pre-exponential factor (mol·m^{-2}·s^{-1}), R is a gas constant (8.31 J·mol^{-1}·K^{-1}), T is the soil temperature, S is the reactive surface (m^2), a_{H^+} is the proton activity, aO_2 is the dissolved oxygen activity, n is the reaction order, and (1-Q/K) is the saturation index.

For carbonate minerals, in basic conditions, Equation 3 is modified by substituting H^+ activity by pCO_2. All kinetic parameters are explained in Palandri and Kharaka (2004). Precipitation rate data do not exist for most minerals, because in mineral precipitation experiments, undesired metastable reaction products usually precipitate instead of the more stable mineral, especially when the conditions are far from equilibrium at a high degree of supersaturation.

The modelling was performed using (a) the mineral assemblage and the chemical composition of the black marls; (b) the chemical and physical properties of the starting solution (e.g., rainfall); and (c) the thermodynamic data, reactive kinetics and reactive surfaces of the mineral phases:

1. The modal composition of the black marls, which is based on the mineralogical and geochemical analyses described previously, was used to obtain the stoichiometry of the solid reactants. Uncertainties remain on the actual proportion of some minerals. This is mainly the case for pyrite, which is not clearly detected in the mineralogical analyses, although observed in the field. Pyrite alteration is a major process for sulphate production in the liquid phase, and the model is very sensitive to the proportion of pyrite in the initial material. The simulations are performed with a proportion of pyrite ranging from 0.1% to 2.0%. According to the previous works of Malet (2003) and de Montety et al. (2007) at Super-Sauze and Garel et al. (2010) at Draix-Laval, a mean porosity of 25% is taken into account for the field-scale simulations. In the case of the leaching simulation, all the water interacts with 50 g of crushed soil with a porosity considered equal to 100%.
2. In first approximation, the initial water used to simulate the *in situ* groundwater chemistry consisted in a weighted average composition of rainwaters collected at the sites. The weighting mean value by rainfall amount was calculated from five rainwater samples. Initial pH was 5.8, and initial temperature was 10°C. An open system continuously exchanging oxygen with the atmosphere is considered ($logpCO_2$ = −3.5, $logpO_2$ = −0.68). This assumption means that CO_2 (together with oxygen) diffuses continuously to the groundwater thanks to open fractures and pores, providing the necessary acid for the neutralization of the base generated through the dissolution of clay minerals. Snowmelt water may have slight chemical differences with rainwater (less exchange with CO_2, higher adsorption capacity for atmospheric dust). The use of snowmelt water instead of rainwater in the model is assumed nonrelevant considering the expected low chemical differences and the final groundwater solutes concentration (around 1,000 times higher than the input water chemical content).
3. Kinetic laws are considered for a neutral environment, as the pH is close to 7. In a first approximation, the reactive surfaces are estimated using the formula proposed by Murphy and Helgeson (1989). Considering the grain shape as spherical, the reactive surface Sp (cm^2·g^{-1}) is calculated with (Equation 4). The mean diameter of the grain for all the mineral phases was obtained from the scientific literature (de Combarieu et al., 2007):

$$Sp = 6/\sigma.d \quad (4)$$

where σ is the specific density of the mineral (g·cm^{-3}) and d is the diameter of the sphere.

For phyllosilicate minerals, the reactive surfaces are estimated from Santamarina et al. (2002) and Lérau (2013).

4 | RESULTS

4.1 | Soil leaching

4.1.1 | Hydrochemical features

Results from the leaching experiments are summarized in Table 2. For all waters, the hydrochemical facies is dominated by calcium and sulphate. Magnesium content is also meaningful but significantly lower than calcium (−30% to −50%). The other ions have a minor impact on the total mineralization (e.g., sodium). As the experimental conditions were similar for all the samples, the large variation of sulphate concentration between the different samples can only be explained by the heterogeneous distribution of pyrite in the soil. This impact is reduced for calcium and magnesium concentrations, as they are mainly involved in carbonate dissolution.

4.1.2 | Geochemical modelling

The simulations are compared using the efficiency coefficient EI (error index), which assesses the differences between the observed concentration (*Cobs*) for the n compounds and the model outputs (*Ccalc*) (Equation 5)

TABLE 2 Chemical content of the water after 10 h of leaching (mmol·l^{-1})

Site	Sample name	SO_4	Ca	Mg	Na
Super-Sauze	BDsoil	0.52	0.74	0.35	0.05
	CPsoil	0.23	0.51	0.28	0.04
	DVsoil	0.10	0.32	0.22	0.02
Draix-Laval	RDC	0.25	0.49	0.36	0.03
	RGC	0.09	0.54	0.28	0.03

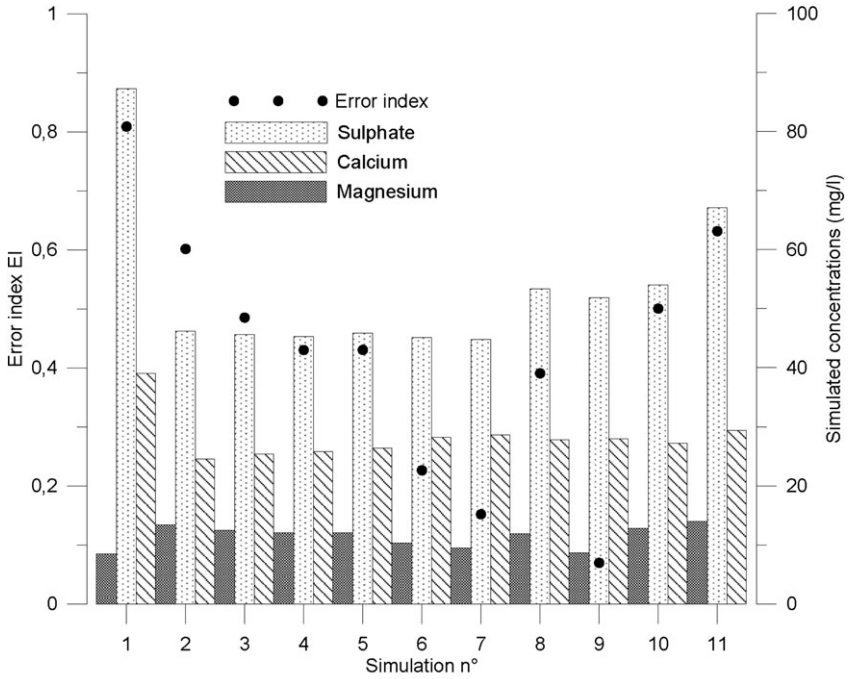

Simulation N°	1	2	3	4	5	6	7	8	9	10	11
Pyrite content (%)	1	0.5	0.5	0.5	0.5	0.5	0.5	0.6	0.6	0.6	0.75
Reactive surface Calcite (% of initial value)	100	10	10	10	20	20	20	20	20	10	10
Reactive surface Dolomite (% of initial value)	100	1000	400	300	500	200	150	200	100	300	300

FIGURE 5 Modelling water chemistry from leaching experiments in the case of BDSoil sample (Super-Sauze): Simulated concentrations of Ca, Mg, and SO_4 in the leachate for different modelling scenarios and error indices (black dots). The best fitting between measured and simulated concentrations corresponds to the lowest error index

$$EI = \sqrt{\sum_{i=1}^{i=n} \left[\frac{Ccalc_i - Cobs_i}{Cobs_i}\right]^2} \quad (5)$$

Figure 5 presents an example of 11 simulations performed for the leaching results on the BD soil sample. The best simulations for all the samples are detailed in Table 3. The pyrite proportion required to reproduce the sulphate concentration ranges between 0.1% and 0.6%; these values are significantly lower than the maximum proportion estimated from the mineralogical analyses (2%). The reactive surfaces of calcite and dolomite range, respectively, between 1% and 20% and between 50% and 150% of the initial Sp values. These results are in agreement with the works of Zerai et al. (2006), Xu et al. (2007), and Scislewski and Zuddas (2010). The latter demonstrated by their experimental study that calcite's reactive surface area changed significantly during dissolution by one to two orders of magnitude. The large variations of Sp between the samples can also be explained by the heterogeneity of the soil and the representativeness of the samples.

4.2 | Groundwater chemistry

4.2.1 | Origin of the groundwater chemistry

Water interacting with the black marls shows a high mineralization with a conductivity ranging from 1,500 to 4,500 µs·cm^{-1}. As observed with the leaching experiments, the waters are composed in majority with sulphate, calcium, and magnesium ions (Table 4).

At the Draix-Laval site, the groundwater chemical facies (Figure 6a) and the leached water chemical facies (Figure 6b) are similar and correspond to a SO_4-Ca-Mg type. A small but detectable impact of sodium on the water chemistry is observed in the stream water (drainage of the catchment upwards the landslide; Figure 6a).

At Super-Sauze, the chemical facies of groundwater is changing according to the flow direction from a SO_4-HCO_3 type, without dominant cation to a SO_4-Ca-Mg facies (Figure 6a). The changes in proportion of both cations and anions in the Piper diagram suggest that the facies variation results mainly from material alteration and mineral dissolution. The ion content increases downslope owing to the rise

TABLE 3 Optimized parameters set for all the samples of the leaching experiments

Site	Sample name	Pyrite proportion (%)	Variation of calcite Sp from the initial model (%)	Variation of dolomite Sp from the initial model (%)	Best error index EI	Number of simulations
Super-Sauze	**BDsoil**	**0.6**	**20**	**100**	**0.07**	**11**
	CPsoil	0.25	10	90	0.20	7
	DVsoil	0.125	1	50	0.06	7
Draix-Laval	RGC	0.25	3	150	0.28	11
	RDC	0.3	3	150	0.09	11

Note. In bold is the sample used as illustration of the simulation process in Figure 5.

TABLE 4 Major ions content (mmol·l^{-1}) and water isotopes ratios (‰) in groundwater and surface water at Super-Sauze and Draix-Laval.

		Super-Sauze										
Name	Date	pH	c25°C	HCO_3	SO_4	Cl	NO_3	Na	Ca	Mg	$\delta^{18}O$	$\delta^{2}H$
A6	06/22/2010	7.52	1622	5.3	7.3	n.d.	0.035	7.8	2.5	2.6	−13.42	−95.65
A6	07/21/2010	7.49	1750	5.7	7.6	0.008	0.031	7.2	2.7	3.7	−12.73	−90.32
A6	08/27/2010	7.41	2220	3.1	11.3	0.009	0.018	9.1	4.0	6.1	−12.43	−87.55
A6	10/12/2010	7.14	2570	6.0	12.4	0.012	0.013	10.0	3.5	5.3	−11.75	−82.86
A6	11/27/2010	7.42	2540	5.1	14.2	0.010	0.016	11.8	3.7	5.2	−12.29	−87.93
A6	04/16/2011	7.91	1375	4.6	5.1	0.011	0.037	6.1	1.4	2.2	−13.34	−94.47
A6	05/12/2011	7.86	1174	0.0	3.7	0.019	0.029	4.8	1.3	1.7	−12.95	−91.1
A6	06/10/2011	7.74	1335	4.2	5.7	0.010	0.040	6.3	1.4	2.3	n.d.	n.d.
A6	11/18/2011	7.89	1871	5.5	8.7	0.008	0.035	8.3	2.4	4.4	n.d.	n.d.
BD	06/22/2010	7.57	2410	5.2	15.6	0.044	0.002	13.2	0.3	5.6	−11.56	−81.74
BD	07/21/2010	7.28	3420	6.6	19.1	0.020	n.d.	10.7	0.3	7.5	−11.28	−79.71
BD	08/27/2010	7.21	3630	7.0	23.6	0.038	0.058	13.5	0.4	8.3	n.d.	n.d.
BD	10/12/2010	7.21	3950	6.0	26.0	0.020	0.016	10.0	0.3	8.7	n.d.	n.d.
BD	11/27/2010	n.d.	2290	4.6	22.7	0.011	n.d.	7.5	0.2	8.5	−12.2	−87.56
BD	04/16/2011	n.d.	n.d.	4.2	9.1	0.027	0.011	7.8	0.2	2.7	−13.8	−99.04
BD	05/12/2011	7.72	1508	0.0	9.7	0.028	0.047	9.6	0.1	2.4	n.d.	n.d.
BD	06/10/2011	7.79	1473	2.7	9.1	0.011	0.019	3.6	0.1	3.1	n.d.	n.d.
BD	11/18/2011	8.15	1462	1.9	7.0	0.329	0.088	3.4	0.3	3.0	n.d.	n.d.
BD	07/05/2012	7.91	1976	3.4	10.6	0.072	0.023	6.8	0.2	5.2	n.d.	n.d.
BD	10/06/2012	7.77	3440	3.6	18.4	0.081	0.029	17.9	0.3	4.3	n.d.	n.d.
CP	06/22/2010	7.11	3580	6.0	23.0	0.027	0.004	9.0	9.8	6.1	−12.12	−85.25
CP	07/21/2010	7.16	3450	6.2	21.5	0.024	0.002	9.9	9.0	10.1	−12.1	−85.38
CP	11/27/2010	n.d.	3900	4.8	27.7	0.014	n.d.	6.7	10.8	12.5	−12.68	−91.86
CP	04/16/2011	n.d.	3667	5.5	23.8	0.009	0.007	7.8	9.2	11.1	−12.69	−90.35
CP	05/12/2011	7.11	3690	0.0	24.2	0.016	<0.001	9.0	10.0	12.0	n.d.	n.d.
CP	06/10/2011	7.19	3380	5.7	28.0	0.015	<0.001	7.9	9.1	11.3	n.d.	n.d.
CP	11/18/2011	7.31	4280	6.9	26.2	0.368	<0.001	8.0	9.5	13.8	n.d.	n.d.
CP	07/05/2012	7.11	3930	7.2	22.2	0.056	0.030	9.2	8.7	10.0	n.d.	n.d.
CP	10/06/2012	6.98	3930	8.0	22.9	0.078	0.032	10.7	9.4	11.6	n.d.	n.d.
DV	06/23/2010	7.12	3420	5.6	24.1	0.013	0.022	4.6	9.8	8.2	−11.03	−76.31
DV	07/21/2010	7.16	4230	6.6	27.2	0.021	0.003	5.1	10.9	15.9	−10.78	−75.4
DV	08/27/2010	7.12	4230	7.4	31.1	0.026	n.d.	6.9	11.1	17.1	n.d.	n.d.
DV	11/27/2010	n.d.	2730	4.0	25.6	n.d.	n.d.	2.5	9.5	14.1	−12.18	−87.58
DV	04/16/2011	n.d.	3555	4.7	26.0	n.d.	0.006	3.5	8.8	14.7	−11.81	−84.04
DV	05/12/2011	7.17	3780	0.0	26.6	0.025	<0.001	3.7	10.6	16.5	n.d.	n.d.
DV	06/10/2011	7.09	3890	5.8	31.8	0.016	<0.001	3.8	9.4	16.4	n.d.	n.d.
DV	11/18/2011	7.65	3760	3.3	24.0	n.d.	0.013	2.1	9.5	15.6	n.d.	n.d.
DV	07/05/2012	7.05	3720	5.8	23.1	0.065	0.018	3.0	9.1	13.2	n.d.	n.d.
AS	10/17/2006	7.29	2370	7.64	11.31	0.047	<0.001	7.82	3.1	6.1	n.d.	n.d.
AS	06/29/2013	7.60	2180	7.08	10.32	0.02	0.03	6.64	3.5	5.9	−12.2	−87.59
Name	Date	Draix-Laval										
		pH	c25°C	HCO_3	SO_4			Na	Ca	Mg	$\delta^{18}O$	$\delta^{2}H$
GC	06/21/2010	6.9	3009	6.1	18.8	0.029	<0.001	1.1	8.4	8.5	−9.75	−71.20
GC	07/20/2010	6.88	3380	6.4	21.2	0.014	<0.001	0.6	10.1	12.6	−9.57	−69.98
GC	08/26/2010	6.82	3590	5.7	24.2	0.013	<0.001	0.8	11.4	16.2	−9.73	−42.91
GC	09/29/2010	6.70	3710	7.5	25.0	0.017	n.d.	0.8	12.8	16.7	−9.48	−69.93
GC	11/04/2010	n.d.	n.d.	5.8	23.3	0.013	n.d.	0.5	10.3	12.8	−9.11	−66.35
GC	12/20/2010	n.d.	3330	6.2	20.4	0.014	n.d.	0.6	10.3	12.7	−9.18	−66.47
GC	01/20/2011	7.07	3240	6.0	22.5	0.011	<0.001	0.5	8.3	12.9	−9.07	−66.63
GC	03/02/2011	6.96	3390	6.5	23.3	0.018	n.d.	0.5	9.9	13.3	−9.06	−66.18

(*Continues*)

TABLE 4 (Continued)

		Super-Sauze										
Name	Date	pH	c25°C	HCO_3	SO_4	Cl	NO_3	Na	Ca	Mg	$\delta^{18}O$	$\delta^{2}H$
GC	04/29/2011	6.98	2970	5.8	21.9	0.006	0.005	0.4	8.6	11.7	−9.24	−67.85
L1	06/21/2010	8.15	1761	2.8	9.2	0.35	<0.001	4.1	4.4	3.4	−8.09	−60.63
L1	07/20/2010	7.4	1985	3.6	9.8	0.77	<0.001	4.0	4.6	4.5	−6.98	−54.20
L1	08/26/2010	7.8	2480	2.4	15.1	1.28	<0.001	6.6	6.7	7.3	−6.83	−52.61
L1	09/29/2010	7.84	2290	2.6	13.2	1.23	n.d.	6.5	6.0	6.7	−6.52	−50.21
L1	11/04/2010	n.d.	n.d.	3.5	11.0	0.29	n.d.	4.0	4.4	4.9	−8.35	−61.40
L1	12/20/2010	n.d.	2010	3.6	9.7	0.4	n.d.	4.4	4.5	3.7	−8.55	−62.98
L1	01/20/2011	8.2	1887	3.9	6.6	0.31	<0.001	3.5	3.5	4.2	−8.68	−63.83
L1	03/02/2011	7.92	1874	3.2	20.2	1.55	0.010	9.5	7.4	8.2	−8.26	−60.89
L2	06/21/2010	8.12	1834	3.0	9.4	1.55	<0.001	4.3	4.4	3.4	n.d.	n.d.
L2	07/20/2010	7.8	2050	3.3	10.2	0.34	<0.001	4.7	4.7	5.1	−7.03	−54.63
L2	08/26/2010	7.69	2500	3.6	15.0	0.7	<0.001	6.9	6.7	7.6	−7.26	−54.84
L2	09/29/2010	7.83	2410	3.0	13.9	1.23	n.d.	6.9	6.2	6.8	−6.85	−52.53
L2	11/04/2010	n.d.	n.d.	3.6	11.6	1.14	n.d.	4.2	4.5	5.0	−8.32	−61.26
L2	12/20/2010	n.d.	1990	3.7	9.9	0.29	n.d.	4.5	4.5	3.8	−8.59	−62.94
L2	01/20/2011	8.28	1907	3.8	6.8	0.41	<0.001	4.3	4.1	4.6	−8.66	−63.35
L2	03/02/2011	7.95	1922	3.2	9.8	0.31	n.d.	4.8	4.0	4.5	−8.3	−61.09
L2	04/29/2011	8.03	1654	2.9	9.8	0.76	0.077	2.9	3.7	4.1	−8.4	−61.12
LS	06/21/2010	8.39	1813	2.4	8.4	0.3	<0.001	3.5	4.1	3.8	−7.84	−59.89
LS	07/20/2010	8.23	2350	2.2	13.2	0.53	<0.001	6.6	5.0	5.6	−2.96	−37.90
LS	08/26/2010	8.3	2390	2.4	15.2	0.9	<0.001	5.5	5.6	6.1	−4.73	−42.91
LS	09/29/2010	8.26	2390	2.2	14.6	1.01	n.d.	6.3	5.3	5.9	−5.76	−47.74
LS	11/04/2010	n.d.	n.d.	3.0	11.7	0.25	n.d.	3.8	4.5	5.0	−8.43	−62.20
LS	12/20/2010	n.d.	1933	3.6	9.6	0.39	0.003	4.4	4.3	3.9	−8.64	−63.01
LS	01/20/2011	8.26	1921	3.4	6.9	0.23	<0.001	4.3	4.0	4.7	−8.64	−63.85
LS	03/02/2011	8.15	1817	2.7	9.4	0.59	n.d.	4.5	3.6	4.2	−8.21	−60.88
LS	04/29/2011	8.13	1595	2.9	9.5	0.016	0.071	2.7	3.6	3.9	−8.48	−61.62

Note. n.d. = no data; AS = Argovian spring.

of water residence time with the main water flow lines. Unlike the water from the leaching experiments, the field water chemistry is also influenced by sodium, although no significant content of chloride is detected (Figure 6a and 6c). The sodium content is similar to the calcium or magnesium content in the upper part of the landslide but is decreasing downslope. At Super-Sauze, the groundwater chemical content varies also with time (Figure 7). For sulphate (also calcium and magnesium), the seasonal variation is mainly explained by the impact of water recharge from snowmelt or rainfall events in the spring periods. The lowest concentrations are observed in June owing to the dilution effect caused by the melting of the snow cover. In the A6 area, the sodium concentration increases in autumn and the low concentration in summer results from the dilution with snowmelt water as it was shown with sulphate. Nevertheless, the high concentrations observed (up to 13 meq·l^{-1}) are not in agreement with the mineral phases detected in the material. After the summer period, the increase in sodium concentration in the upper part of the landslide indicates an additional source of water. Sodium shows a different behavior, in the BD area where it is most represented. Unlike the case of the A6 area, the maximum concentration is observed in summer and drops in the autumn and winter seasons. These observations highlight the contribution of an external water in summer without any significant contribution of snowmelt water. This result suggests that the recharge from the external water source occurs according to different modes in the upper part of the landslide (A6 area) and in the BD area.

4.2.2 | Identification of the recharge area

Stable isotopes are used to gain information on the origin of the water. The ^{18}O content of rainfall (expressed in terms of mean annual values) usually decreases with elevation. This property is useful to estimate the mean recharge elevation of the aquifer. The local relation ^{18}O/elevation is difficult to assess as it requires a sampling of rainwater according to the slope and over a long period. This relation is not available at Super-Sauze and at Draix-Laval but was established at the La Clapière landslide situated 25 km from Super-Sauze and 46 km from Draix. Snowmelt contributes greatly to the recharge of the ephemeral springs used for establishing the isotope gradient at La Clapiere. This impact of snowmelt is also observed at Super-Sauze. The experimental relationship proposed for summer and winter at La Clapière (Gugliemi et al, .2000) has a slope close to the reference curves established for the Mediterranean region (between 0.15% and 0.30‰ 100 m^{-1}; Guglielmi et al., 1998; Novel et al., 1999; Celle et al., 2000).

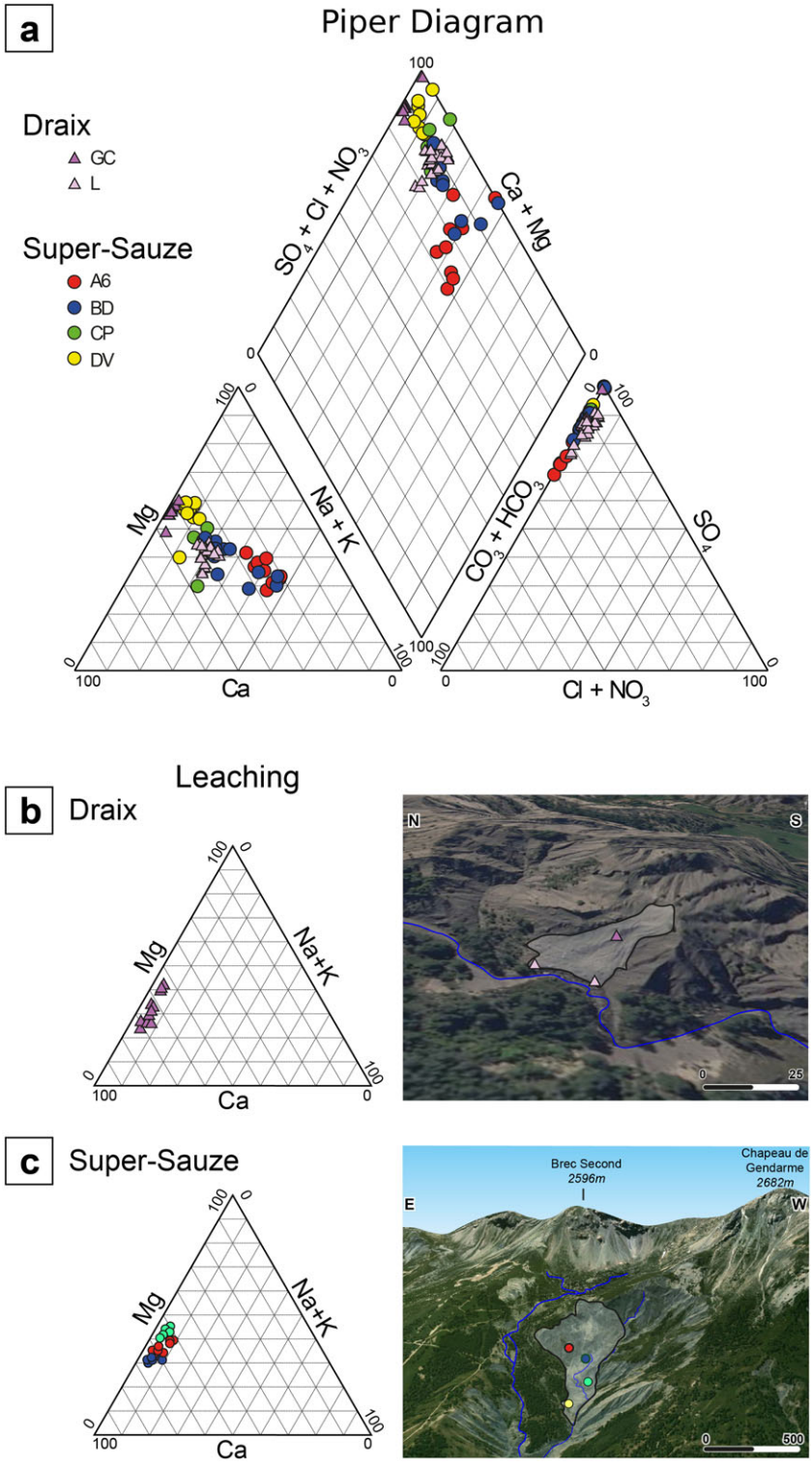

FIGURE 6 Chemical facies of the Super Sauze and Draix groundwater in a piper diagram (a). Trilinear diagram of cations from the leaching experiments and location of the samples on the field for the Draix soils (b) and the Super-Sauze soils (c). Colors of the dots in the trilinear diagrams refer to the position of the samples on the field

Figure 8a compares the mean $\delta^{18}O$ in groundwater to the expected values from the relationship by Guglielmi et al. (2000). The mean values are calculated from water sampled over 1 year. The plot indicates that the mean ^{18}O content of groundwater at Super-Sauze is lower than the one predicted by the regional gradient. The measured values reported in Figure 8a show that the variations around the mean value can be more than 1‰, but all the points are below the winter curve for the transects A and C. These depleted values show that the recharge area is significantly higher than the sampling elevation. At Draix-Laval, the ^{18}O content of the shallow groundwater is in agreement with the prediction indicating that the water recharge occurs locally. Isotope data on surface water are far more enriched than model predictions. On a $\delta^{2}H$ versus $\delta^{18}O$ plot, the surface water samples collected in summer are below the local meteoric water line (Figure 8b). This suggests that the ^{18}O and ^{2}H contents of surface waters are mainly influenced by local rainwater during the flood events and by evaporation processes over the dry period.

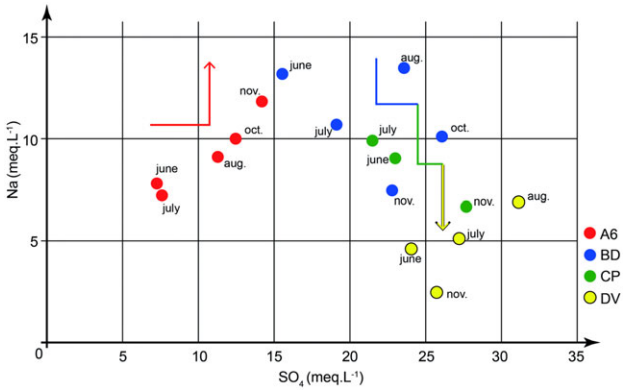

FIGURE 7 Variation over time and area of SO_4 and Na in the groundwater at Super-Sauze

4.2.3 | Water-rock interaction modelling

As for the leaching experiments, PHREEQC is used to simulate the observed concentrations in the groundwater. In a first attempt, simulations are performed with an initial rainwater and using the original geochemical and mineralogical information from the laboratory analyses. Pyrite proportion is 2%. Figure 9a presents the modelling results for Ca, Mg, and SO_4 compared with the observed data at Super-Sauze. As previously noted, the variation in time of the water chemical content is due to changes in the recharge conditions (dilution by infiltration of rain and snowmelt waters). The rising concentration, according to the main water flow directions, is the consequence of an increasing contact time of water with the soil. This first simulation shows that the model underestimates Mg content and overestimates Ca content.

The water-rock interactions are then simulated by using the results of the leaching experiments. At Super-Sauze, the proportion of pyrite is reduced to 0.6%; the reactive surface of calcite represents 20% of the calculated value using the Murphy and Helgeson model (Murphy and Helgeson, 1989). The reactive surface of dolomite is unchanged. Figure 9b indicates that the model outputs are improved, although the Mg content is overestimated. These simulations validate the parameterization of the model from the leaching data (respective proportion of pyrite, calcite, and dolomite). In order to enhance the quality of geochemical modelling at Super-Sauze, a third set of simulations is carried out by modifying the nature of the initial water. The results are presented in Figure 9c for an initial water sampled at a spring above the landslide. This spring drains a part of the rocky massif above the landslide; this massif is made up of different formations comprising Argovian marls and several limestone series. The water from the spring is flowing at the contact between the Argovian marls and the underlying Callovo-Oxfordian black marls.The spring water chemistry is dominated by sulphate (11 mmol·l^{-1}), sodium (7 mmol·l^{-1}), and to a lesser extent magnesium (6 mmol·l^{-1}) and calcium (3 mmol·l^{-1}; see Table 4). Figure 9c shows that the use of the argovian springwater as model input improves significantly the simulations for Mg content, but Ca content is underestimated. These results indicate that groundwater recharge occurred both from the direct infiltration of local rainfall and from water sources situated on the landslide.

The same modelling approach is used for the Draix-Laval landslide. A first set of simulations with the original mineralogical parameters (2% of pyrite) indicates that simulated concentrations are underestimated for magnesium and overestimated for calcium (Figure 10a). The pyrite proportion is thus modified with the reactive surfaces of calcite and dolomite obtained from the leaching experiments. The pyrite proportion is 0.25%, the reactive surface of calcite is 3% of the initial value estimated with the Murphy and Helgeson model, and the reactive surface is 150% of the initial estimation. Figure 10b shows a good fit between the simulated and observed values. Nevertheless, two samples with the highest observed concentrations in magnesium are not correctly simulated, while a good fit is obtained for calcium concentrations. These samples were collected in August and September; the anomalous magnesium concentration for these two dates are explained by the leaching of a $MgSO_4$ salt following summer storms.

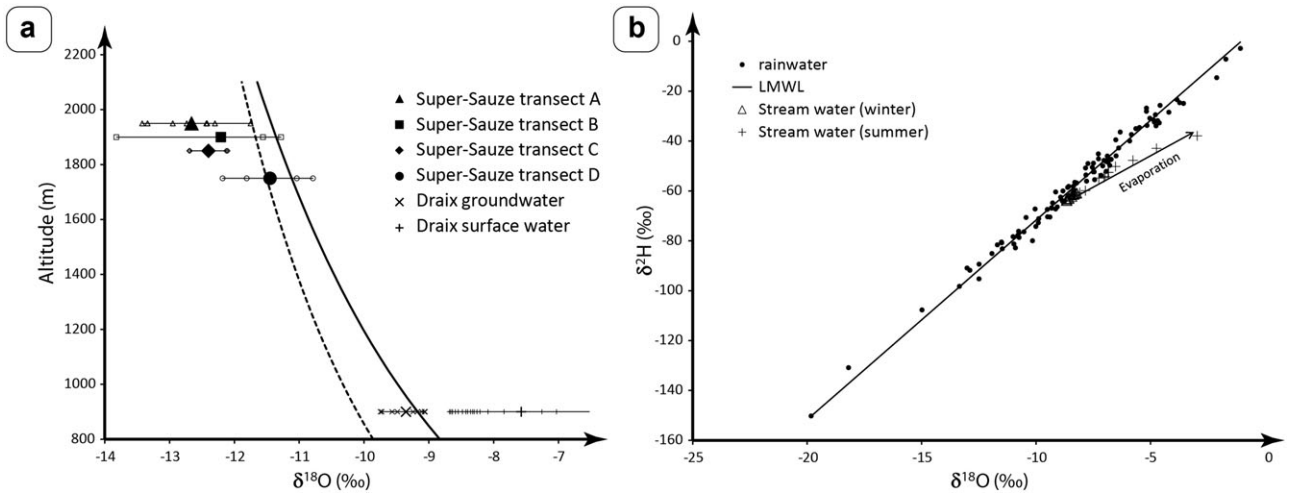

FIGURE 8 (a) Plots of $\delta^{18}O(H_2O)$ versus altitude for water from Super Sauze landslide and Draix-Laval catchment. Mean values (large black symbols) are represented with the seasonal samples (in small symbols). The isotopic gradients (dashed line: summer; continuous line: winter) was obtained by Guglielmi et al. (2000) for the La Clapiere landslide. Calibration springs had been sampled during July 1996 (snowmelt period) and December 1995. (b) δ^2H versus $\delta^{18}O$ in rainwater (over the period 2004–2013 from the Global Network of Isotopes in Precipitation (GNIP) database, LMWL: local meteoric water line) and in the Laval streamwater

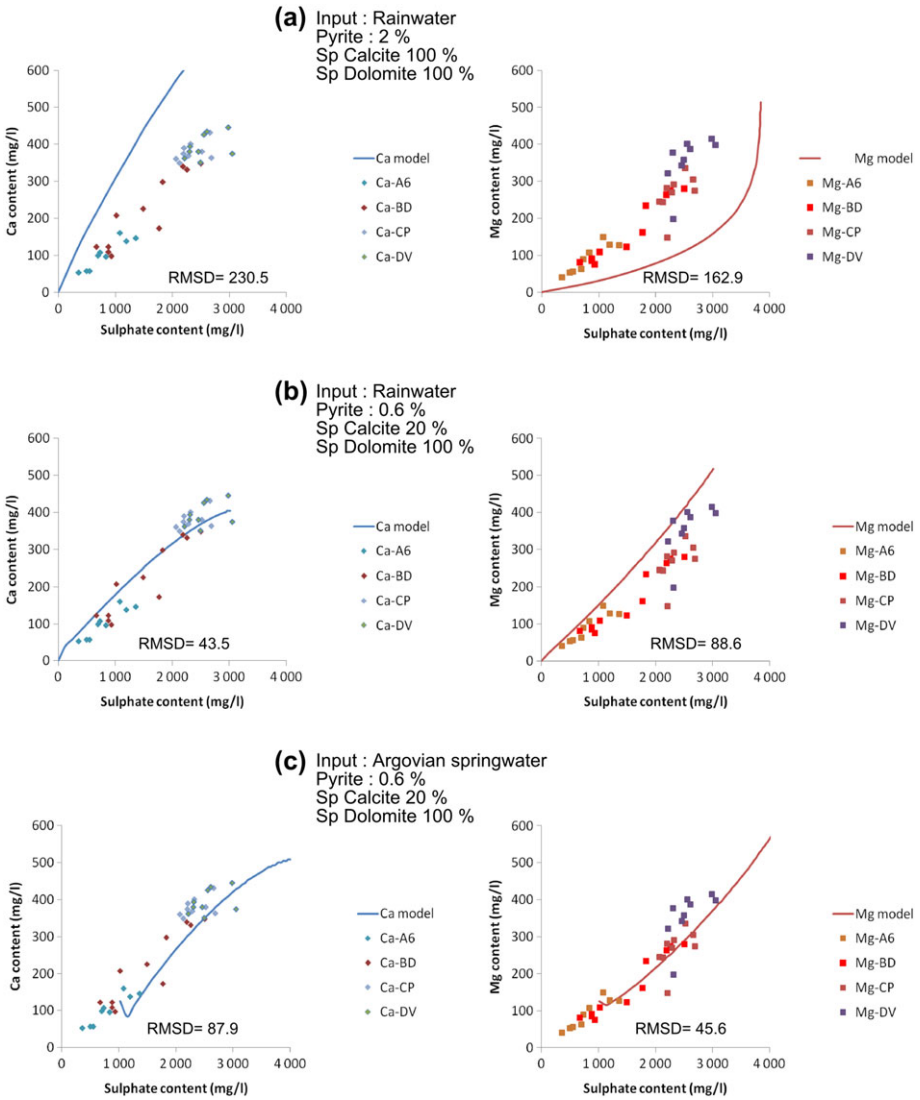

FIGURE 9 Observed and simulated groundwater chemistry at Super-Sauze (Ca and Mg vs. SO_4; RMSD: root mean square deviation)

$MgSO_4$ precipitation from the evaporation of soil water is indeed observed every summer at the soil surface (Cras, 2005). Unlike at Super-Sauze, the groundwater chemistry at Draix-Laval can thus only be explained by local recharge and rainwater-rock interactions.

5 | CONCEPTUAL MODELS OF LANDSLIDE GROUNDWATER FLOW SYSTEMS

5.1 | Conceptual groundwater flow system at Super-Sauze landslide

At Super-Sauze, the major sodium anomaly observed in the upper part of the landslide is not in agreement with the mineralogical bulk. The only mineral phases containing sodium are Na-Feldspar (albite) and Na-montmorillonite (smectite). Such minerals are not expected to provide large concentrations in sodium like those observed *in situ*. As indicated by the sodium-enriched spring-water at the top of the landslide, the origin of sodium is clearly outside of the landslide area. Furthermore, isotope data indicate that the recharge area is far higher than the maximum elevation of the landslide. These two independent analyses evidence the external supply of water out of the landslide. This is also confirmed by the geochemical modelling highlighting that water chemistry could be simulated by water-rock interactions taking into account an initial water solution representative of the Argovian spring-water.

High soluble materials, such as evaporitic facies, can be found at the basement of the klippe of Lan, especially in the Triassic formations (see Section 2.2).

Figure 11 presents a tentative conceptual model of the Super-Sauze landslide groundwater flow system. A regional hydrogeological system develops from the klippe of Lan, which can be considered as a water tower (I). The abnormal contact of allochthonous series with the autochthonous black marls creates a hydraulic barrier, which favor water storage (II). The dissolution of the Triassic evaporitic series consisting of high solubility minerals results in a sharp increase of total dissolved solids before the drainage of water downslope through the upper Cretaceous meridian faults system crossing the autochthonous units (III). This water is supposed to contribute to the recharge of the landslide groundwater in the upper part of the landslide. On the A6 area, the hydrochemical data indicates that the impact of this external water on the landslide groundwater chemistry rises during low flow

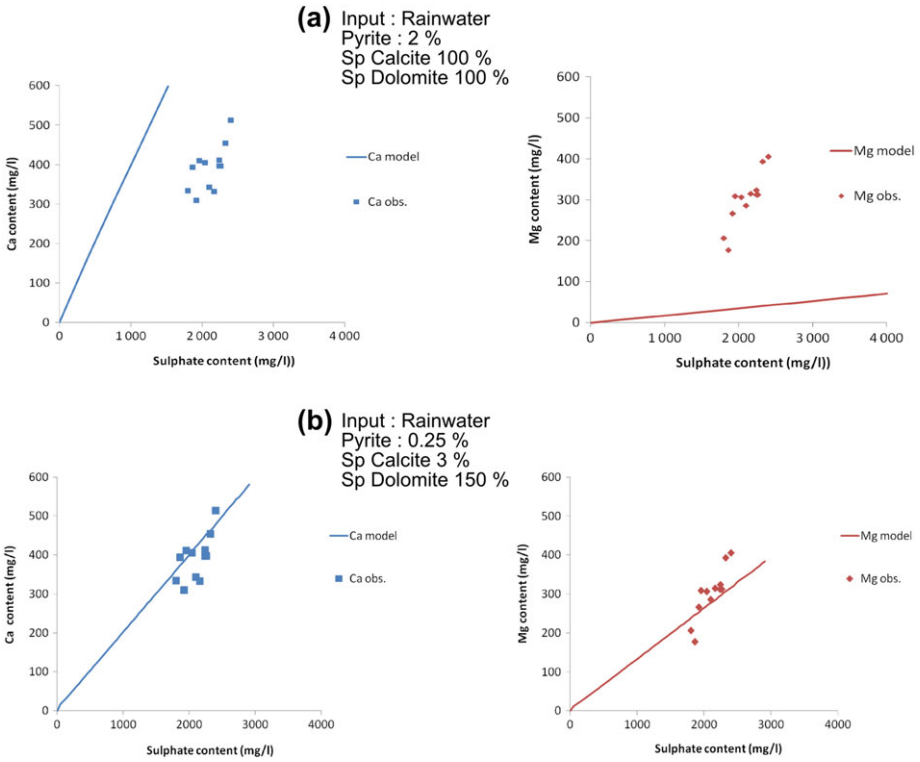

FIGURE 10 Observed and simulated groundwater chemistry at Draix-Laval (Ca and Mg vs. SO_4)

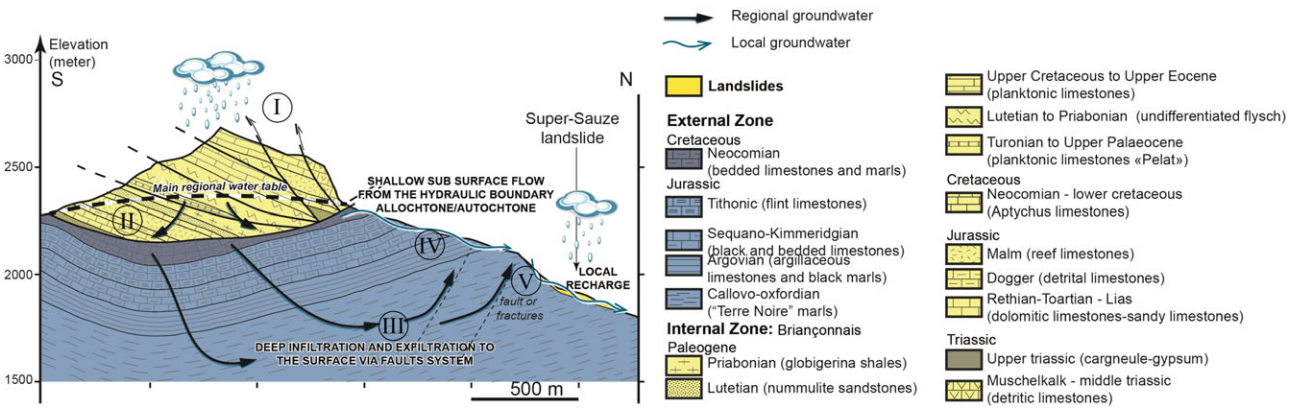

FIGURE 11 Conceptual model of the hydrogeological system at Super-Sauze

periods (autumn) and decreases in summer after the snowmelt. This observation suggests a continuous and superficial origin of this external water because water dilution (by the direct infiltration of rain and snowmelt water) is detected (IV). On the B area, the high concentration in sodium during the summer periods proves that different hydrological processes occur. The post-snowmelt recharge periods have a regional scale influence and result in a rise of the hydraulic head in the aquifers (even in the klippe of Lan system). The landslide aquifer, below the B sector, is probably recharged from a deep, preferential flow-path (active role of the Cretaceous fault system) whose influence decreases as the hydraulic head lowers (autumn season; V).

All over the extent of the landslide, dilution by oxidizing rainwater is a favorable factor for pyrite alteration producing protons used for carbonates dissolution. Consequently, SO_4, Ca, and Mg contents increase downslope as indicated in Figure 6a. Carbonate alteration by pyrite oxidation was already described in different lithological and climatological contexts (Gaillardet et al., 1999; Beaulieu et al., 2011; Dongarrà et al., 2009; Vallet et al., 2015).

5.2 | Conceptual groundwater flow system at Draix-Laval landslide

At Draix-Laval landslide, no hydrochemical anomaly is observed in the shallow groundwater. The isotope content is in agreement with the regional model of isotope distribution with elevation (Guglielmi et al., 2000). The geochemical modelling suggests that groundwater chemistry can be fully explained by the interaction between the soil and the rainwater. The major part of the recharge of the shallow groundwater system consists of local infiltration of rainwater (Figure 12; I). However, stream water is more enriched in sodium than shallow

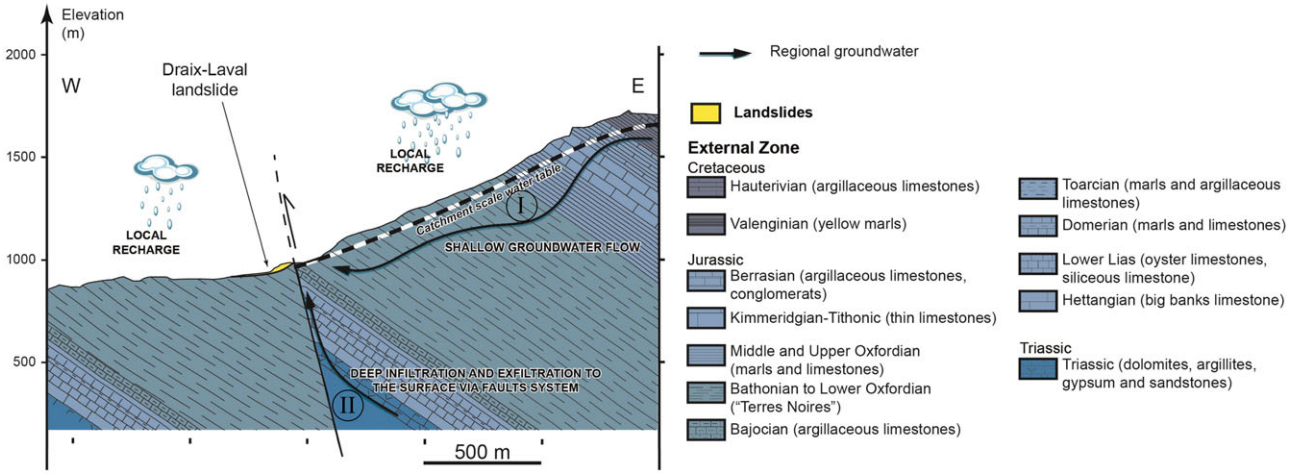

FIGURE 12 Conceptual model of the hydrogeological system at Draix-Laval

groundwater. As for the Super-Sauze landslide, this anomaly in sodium points out the influence of a deep water source at the catchment scale. The Laval catchment is crossed by the Col de la Cine meridian dextral strike-slip fault dated from Oligocene. Triassic evaporite facies are observed along this major fault in depth. A deep drainage of water (II) occurs nearby the fault, resulting in a high sodium content in the river water. In the same area, Lofi et al. (2012) used borehole geophysics, and artificial tracing to demonstrate that water flows through open faults in the black marls bedrock can be observed. The impact of this deep water flow in the fault system is mostly detected in the river during low flow periods.

6 | DISCUSSION

6.1 | Impacts of bedrock and surficial groundwater systems on slope stability

At Super-Sauze, the slip surface is about 20-m deep. Previous studies showed that rainwater or snowmelt water could infiltrate through the soil, possibly using preferential pathways such as the crack network induced either by the soil deformation (Stumpf et al., 2012) or by swelling–shrinking processes affecting clay minerals (Debieche et al., 2012; Krzeminska et al., 2012). All these processes assumed an impervious bedrock. The groundwater chemistry (Figures 6 and 7) and the isotope analyses (Figure 8) allowed proposing a conceptual model where the shallow (e.g., local) groundwater system is superimposed to the bedrock (e.g., regional) system developed from the klippe of Lan (Figure 11). This situation assumes a groundwater outflow through the bedrock from a set of active fractures. Thus, an upward flow in the upper part of the landslide will result in a rise of the hydraulic head and a higher gradient of water head than anywhere else in the aquifer system. As Binet et al. (2007) stated, "even if the slip surface is developing in a same material, it plays a role of discontinuity for groundwater flow with a rise of porosity and hydraulic conductivity." This upward water inflow can result in large ranges of pore water pressure built up below the slip surface but can also act as fluid facilitating the sliding.

At Draix-Laval, groundwater chemistry did not reveal any anomaly during the observation period, suggesting that groundwater recharge occurs mainly from local rainwater (Figures 6, 8, 10, and 12). However, at the scale of the hydrological catchment, an upward deep outflow via a regional major fault is detected in the stream (Figure 6).

Consequently, water outflows from the bedrock (as observed at Super-Sauze and Draix-Laval) suggest that this hydrological situation could be common in black marls slopes in tectonized region such as the Alpine area.

6.2 | Impact of pore water chemistry on the clayey soil structure and the mechanical parameters

Dilute water results in a reduction of shear strength (Moore and Brunsden, 1996; Di Maio et al., 2004, 2014; Picarelli et al., 2006), especially for material in which smectite is the dominant clay mineral and in which Na is progressively substituted by Ca on the clay surface. Thus, if the total ionic concentration of water is increasing, shear strength and soil stability increase. However, the ionic strength of the solution is not the unique factor explaining clay sensitivity. The relative concentration of the different elements, according to the mineralogy (Bogaard et al., 2007) or to the total concentration (Andersson-Skold et al., 2005), has also to be considered.

In black marls slopes, total dissolved solids in groundwater can reach values higher than 5 $g{\cdot}l^{-1}$ and lower than 0.2 $g{\cdot}l^{-1}$ when dilution occurs during rainwater infiltration. At Draix-Laval where the proportion of interstratified illite/smectite reaches 30%, rainwater can infiltrate through the surficial crack systems and contribute to the drop of material cohesion by leaching pore water and promoting inter-particle repulsion. At Super-Sauze, this process has a minor impact because of the low proportion of smectite (less than 5%) in the media. However, the high sodium content observed in the pore water (mean value up to 10 $mmol{\cdot}l^{-1}$ and a maximum of 18 $mmol{\cdot}l^{-1}$) results in a rise of sodium in the clay-humic complex, which, in turn, triggers the dispersion of clay particles (Saidi et al., 2004). This disaggregation leads to a decrease of shear strength but also to an enhanced mobility of the clay particles contributing to the clogging of pores and the drop of hydraulic conductivity. The formation of impervious layers inside the soil mass can thus provoke the increase of pore water pressures and trigger slope instability.

6.3 | Future investigations

The hydraulic conductivity of the soil units and the hydraulic gradients are first-order factors controlling slope instability. However, the estimation of water pressures requires a more detailed knowledge of the hydraulic head distribution than the one currently integrated in landslide hydrological models (Malet et al., 2005; Bogaard and Greco, 2016). At Super-Sauze, the knowledge of hydraulic heads variation is limited to the shallow part of the landslide (<4 m). A set of variable-depth boreholes till the bedrock are necessary to measure vertical hydraulic gradients and detect deep flows through the bedrock.

Weathering of the black marls material result in strength regain on the long-term because of the increase of the residual angle of friction (Maquaire et al., 2003) in relation to the chemical alteration of the clay minerals. This result is independent of the pore water chemistry, which was not investigated in this work. Assuming a constant pore water chemistry concentration, the black marls material is becoming more stable with time but this situation may change in case of transient variations of pore water chemistry according to changes in the recharge conditions. We thus hypothesize that some of the landslide conditioning factors can be related to grain-scale processes, such as a gradual modification of the hydrological properties by pore clogging or changes in electrostatic strengths by variations in the pore water chemistry. Further laboratory investigations are required to specify, for different materials, the role of water-rock interactions in the processes affecting the material cohesion. Information is required on the changes of soil porosity and hydraulic conductivity with dissolution/precipitation of the soluble mineral phases and with the pore water quality affecting the stability of clay minerals.

7 | CONCLUSION

Groundwater-surface waters interactions at slope and catchment scales and their implications for landsliding in clay-rich slopes have been investigated in two experimental sites in the Southern Alps. At Super-Sauze, field and laboratory hydrogeochemical investigations confirmed that hydrochemical anomalies were explained by the contribution of the bedrock groundwater system to the local hillslope groundwater flow. This external water flow occurs in the upper part of the landslide at the contact between the black marls and the overlying formations, or at the landslide basement via a fault network. In both cases, the result is an increase of the hydraulic head in the system increasing slope instability. The presence of evaporites at the basement of the klippe of Lan topping the landslide provides Na-enriched waters, which are suspected to promote weathering of the marls by the dispersion of clays. At Draix, groundwater recharge in the Laval landslide occurs only from local rainwaters; however, a catchment scale analysis indicates that deep groundwater flows participate to the low discharge flows in the river.

Interactions between multi-scale hydrogeological systems are relevant in mountainous areas and can be an additional factor for slope instability in already fragile environments (steep slopes, alteration-prone material). Many questions remain about the way these deep flows contribute to the landslide dynamics. For instance, further investigations are needed to assess the impact of the deep water chemistry on the black marls geotechnical resistance. Active geochemical processes such as pyrite oxidation and carbonate dissolution control the chemical alterability of the black marls.

ACKNOWLEDGEMENTS

This work was supported through the SISCA Project within the 2009–2011 ANR Risknat program of research and by the EU Safeland project within the 7th Framework program of research. We acknowledge the OMIV (Observatoire Multidisciplinaire des Instabilités de Versants) National Observation Service and the GIS (Groupement d'Intérêt Scientifique) Draix-Bléone for their technical support and their ongoing maintenance of the experimental sites. Constructive remarks provided by two anonymous reviewers were appreciated as they allowed to greatly improve an earlier version of the manuscript.

REFERENCES

Andersson-Skold, Y., Torrance, J. K., Lind, B., Oden, K., Stevens, R. L., & Rankka, K. (2005). Quick clay—A case study of chemical perspective in Southwest Sweden. *Engineering Geology*, *82*, 107–118.

Appelo, C. A. J., Vinsot, A., Mettler, S., & Wechner, S. (2008). Obtaining the porewater composition of a clay rock by modeling the in- and out-diffusion of anions and cations from an *in-situ* experiment. *Journal of Contaminant Hydrology*, *101*, 67–76.

Beaucaire, C., Michelot, J.-L., Savoye, S., & Cabrera, J. (2008). Groundwater characterization and modelling of water–rock interaction in an argillaceous formation (Tournemire, France). *Applied Geochemistry*, *23*, 2182–2197.

Beaulieu, E., Goddéris, Y., Labat, D., Roelandt, C., Calmels, D., & Gaillardet, J. (2011). Modeling of water-rock interaction in the Mackenzie basin: Competition between sulfuric and carbonic acids. *Chemical Geology*, *289*, 114–123.

Bense, V. F., Gleeson, T., Loveless, S. E., Bour, O., & Scibek, J. (2013). Fault zone hydrogeology. *Earth Science Reviews*, *127*, 171–192.

Binet, S., Jomard, H., Lebourg, T., Guglielmi, Y., Tric, E., Bertrand, C., & Mudry, J. (2007). Experimental analysis of groundwater flow through a landslide slip surface using natural and artificial water chemical tracers. *Hydrological Processes*, *21*, 3463–3472.

Bogaard, T. A., & Greco, R. (2016). Landslide hydrology: From hydrology to pore pressure. *Wiley Interdisciplinary Reviews*, *3*(3), 439–459.

Bogaard, T. A., Guglielmi, Y., Marc, V., Emblanch, C., Bertrand, C., & Mudry, J. (2007). Hydrogeochemistry in landslide research: A review. *Bulletin de la Société Géologique de France*, *178*, 113–126.

Bonzanigo, L., Eberhardt, E., & Loew, S. (2001). Hydromechanical factors controlling the creeping Campo Vallemaggia landslide, in: Proceeding of landslides-causes, impacts and countermeasures, Davos, Switzerland. 13–22.

Borgès, A.L.d.O., (1993). Modélisation de l'érosion sur deux bassins versants expérimentaux des Alpes du Sud, (Ph.D thesis), Université Joseph Fourier—Grenoble I, Grenoble, 205 p.

Brunsden, D. (1999). Some geomorphological considerations for the future development of landslide models. *Geomorphology*, *30*, 13–24.

Calmels, D., Galy, A., Hovius, N., Bickle, M., West, A. J., Chen, M.-C., & Chapman, H. (2011). Contribution of deep groundwater to the weathering budget in a rapidly eroding mountain belt, Taiwan. *Earth and Planetary Science Letters*, *303*, 48–58.

Cappa, F., Guglielmi, Y., Merrien-Soukatchoff, V., Mudry, J., Bertrand, C., & Charmoille, A. (2004). Hydromechanical modeling of a large moving rock slope inferred from slope levelling coupled to spring long-term hydrochemical monitoring: Example of the La Clapière landslide (Southern Alps, France). *Journal of Hydrology*, *291*, 67–90.

Celle, H., Daniel, M., Mudry, J., & Blavoux, B. (2000). Signal pluie et traçage par les isotopes stables en Méditerranée occidentale. Exemple de la

région avignonnaise (Sud-Est de la France). Comptes Rendus de l'Académie des Sciences—Series IIA—Earth and. *Planetary Science*, *331*, 647–650.

Cervi, F., Ronchetti, F., Martinelli, G., Bogaard, T. A., & Corsini, A. (2012). Origin and assessment of deep groundwater inflow in the Ca'Lita landslide using hydrochemistry and *in situ* monitoring. *Hydrology and Earth System Sciences*, *16*, 4205–4221.

Cras, A., (2005). Etude des mécanismes de transfert d'eau et d'éléments sur bassins versants torrentiels marneux (BV de Draix, Alpes de Haute Provence). Apport du couplage des méthodes hydrométriques, de la géochimie isotopique et de la modélisation hydrologique. PhD Thesis, Université d'Avignon et des Pays de Vaucluse, Avignon, 161p.

De Combarieu, G., Barboux, P., Minet, Y., (2007). Iron corrosion in Callovo–Oxfordian argilite: From experiments to thermodynamic/kinetic modelling. Physics and Chemistry of the Earth, Parts A/B/C, Clay in natural and engineered barriers for radioactive waste confinement—Part 1 32, 346–358.

de Graciansky, P. C. (1972). Le bassin tertiaire de Barrême (Alpes de Haute-Provence): Relations entre déformation et sédimentation; chronologie des plissements. *Comptes Rendus de l'Académie des Sciences*, *275*, 2825–2828.

de Montety, V., Marc, V., Emblanch, C., Malet, J. P., Bertrand, C., Maquaire, O., & Bogaard, T. A. (2007). Identifying the origin of groundwater and flow processes in complex landslides affecting black marls: Insights from a hydrochemical survey. *Earth Surface Processes and Landforms*, *32*, 32–48.

Debieche, T.-H., Bogaard, T. A., Marc, V., Emblanch, C., Krzeminska, D. M., & Malet, J.-P. (2012). Hydrological and hydrochemical processes observed during a large-scale infiltration experiment at the Super-Sauze mudslide (France. *Hydrological Processes*, *26*, 2157–2170.

Di Maio, C., Santoli, L., & Schiavone, P. (2004). Volume change behaviour of clays: the influence of mineral composition, pore fluid composition and stress state. *Mechanics of Materials*, *36*, 435–451.

Di Maio, C., Scaringi, G., & Vassallo, R. (2014). Residual strength and creep behaviour on the slip surface of specimens of a landslide in marine origin clay shales: influence of pore fluid composition. *Landslides*, 1–11.

Dongarrà, G., Manno, E., Sabatino, G., & Varrica, D. (2009). Geochemical characteristics of waters in mineralised area of Peloritani Mountains (Sicily, Italy. *Applied Geochemistry*, *24*, 900–914.

Epstein, S., & Mayeda, T. (1953). Variation of O18 content of waters from natural sources. *Geochimica et Cosmochimica Acta*, *4*, 213–224.

Esteves, M., Descroix, L., Mathys, N., & Lapetite, J.-M. (2005). Soil hydraulic properties in a marly gully catchment (Draix, France. *Catena*, *63*, 282–298.

Flageollet, J.-C., Malet, J.-P., & Maquaire, O. (1999a). The 3D structure of the Super-Sauze earthflow: A first stage towards modelling its behaviour. *Physics and Chemistry of the Earth*, *25*(9), 785–791.

Flageollet, J. C., Maquaire, O., Martin, B., & Weber, D. (1999b). Landslides and climatic conditions in the Barcelonnette and Vars basins (Southern French Alps, France. *Geomorphology*, *30*, 65–78.

Forster, C. B., & Evans, J. P. (1991). Fluid flow in thrust faults and crystalline thrust sheets: Results of combined field and modeling studies. *Geophysical Research Letters*, *18*, 979–982.

Fressard M (2008) Le glissement de terrain du Laval Morphologie-Evolution-Cartographie (Draix, Alpes de Haute Provence, France), Mémoire de Master 1, Université de Caen Basse-Normandie, Caen, p.156

Gaillardet, J., Dupré, B., Louvat, P., & Allègre, C. J. (1999). Global silicate weathering and CO_2 consumption rates deduced from the chemistry of large rivers. *Chemical Geology*, *159*(1–4), 3–30.

Garel, E., (2010). Etude des processus de recharge des nappes superficielles et profondes dans les versants marneux fortement hétérogènes. Cas des Terres Noires des Alpes du Sud de la France—ORE Draix. Ph.D Thesis, Université d'Avignon et des Pays de Vaucluse, Avignon, 159 p.

Garel, E., Marc, V., Ruy, S., Cognard-Plancq, A.-L., Klotz, S., Emblanch, C., & Simler, R. (2012). Large scale rainfall simulation to investigate infiltration processes in a small landslide under dry initial conditions: The Draix hillslope experiment. *Hydrological Processes*, *26*, 2171–2186.

Gaucher, É. C., Blanc, P., Bardot, F., Braibant, G., Buschaert, S., Crouzet, C., … Altmann, S. (2006). Modelling the porewater chemistry of the Callovian–Oxfordian formation at a regional scale. *Comptes Rendus Geosciences*, *338*, 917–930.

Gaus, I., Azaroual, M., Czernichowski-Lauriol, I., (2005). Reactive transport modelling of the impact of CO2 injection on the clayey cap rock at Sleipner (North Sea). Chemical Geology, Geochemical Aspects of CO2 sequestering Geochemical Aspects of CO2 sequestering 217, 319–337.

Goldscheider, N., & Neukum, C. (2010). Fold and fault control on the drainage pattern of a double-karst-aquifer system, Winterstaude, Austrian Alps. *Acta Cardiologica*, *39*, 173–186.

Gran, G. (1952). Determination of the equivalence point in in the potentiometric titrations. *Analyst*, *77*, 661–671.

Guglielmi, Y., Mudry, J., & Blavoux, B. (1998). Estimation of the water balance of alluvial aquifers in region of high isotopic contrast: an example from southeastern France. *Journal of Hydrology*, *210*, 106–115.

Guglielmi, Y., Bertrand, C., Compagnon, F., Follacci, J. P., & Mudry, J. (2000). Acquisition of water chemistry in a mobile fissured basement massif: its role in the hydrogeological knowledge of the La Clapiere landslide (Mercantour massif, Southern Alps, France). *Journal of Hydrology*, *229*, 138–148.

Haccard, D., Beaudoin, B., Gigot, P., Jorda, M., (1989). Notice explicative, carte géol. France (1/50000), feuille LA JAVIE (918). BRGM, Orléans.

Iverson, R. M. (2000). Landslide triggering by rain infiltration. *Water Resources Research*, *36*, 1897–1910.

Iverson, R. M., & Major, J. J. (1986). Groundwater seepage vectors and the potential for hillslope failure and debris flow mobilization. *Water Resources Research*, *22*, 1543–1548.

Kerckhove, C., Pairis, J.L., Plan, J., (1974). Notice explicative, Carte géol. France (1/50000) feuille Barcelonnette (895). BRGM, Orléans.

Kim, H., Bishop, J. K. B., Dietrich, W. E., & Fung, I. Y. (2014). Process dominance shift in solute chemistry as revealed by long-term high-frequency water chemistry observations of groundwater flowing through weathered argillite underlying a steep forested hillslope. *Geochimica et Cosmochimica Acta*, *140*, 1–19.

Krzeminska, D. M., Bogaard, T. A., van Asch, T. W. J., & van Beek, L. P. H. (2012). A conceptual model of the hydrological influence of fissures on landslide activity. *Hydrology and Earth System Sciences*, *16*, 1561–1576.

Krzeminska, D. M., Bogaard, T. A., Malet, J.-P., & van Beek, L. P. H. (2013). A model of hydrological and mechanical feedbacks of preferential fissure flow in a slow-moving landslide. *Hydrology and Earth System Sciences*, *17*, 947–959.

Lérau J., (2013). Géotechnique, lectures at the Institut National des Sciences Appliquées de Toulouse, year 2005-2006. https://moodle.insa-toulouse.fr/file.php/301/content/jlerau/chapitre_1.pdf

Lofi, J., Pezard, P., Loggia, D., Garel, E., Gautier, S., Merry, C., & Bondabou, K. (2012). Geological discontinuities, main flow path and chemical alteration in a marly hill prone to slope instability: Assessment from petrophysical measurements and borehole image analysis. *Hydrological Processes*, *26*, 2071–2084.

Lüttge, A. (2005). Etch pit coalescence, surface area, and overall mineral dissolution rates. *American Mineralogist*, *90*, 1776–1783.

Malet, J.P., (2003). Les 'glissements de type écoulement' dans les marnes noires des Alpes du Sud. Morphologie, fonctionnement et modélisation hydro-mécanique. (Ph.D thesis), Université Louis Pasteur, Strasbourg, 394 p.

Malet, J.-P., Maquaire, O., & van Asch, T. W. J. (2003). Hydrological behaviour of earthflows developed in clay-shales: investigation, concept and modelling. In L. Picarelli (Ed.), *The Occurrence and Mechanisms of Flows in Natural Slopes and Earthfills*, *Sorrento*, *Italy*, *Patrone Editore*, *Bologna* (pp. 175–193).

Malet, J. P., van Asch, T. W. J., van Beek, R., & Maquaire, O. (2005). Forecasting the behaviour of complex landslides with a spatially distributed hydrological model. Natural Hazards and Earth System. *Science*, *5*, 71–85.

Maquaire, O., Malet, J. P., Remaître, A., Locat, J., Klotz, S., & Guillon, J. (2003). Instability conditions of marly hillslopes: towards landsliding and gullying? The case of the Barcelonnette Basin, South East France. *Engineering Geology*, *70*, 1–2.

Montgomery, D. R., & Dietrich, W. E. (1994). A physically based model for the topographic control of shallow landsliding. *Water Resources Research*, *30*, 1153–1171.

Moore, R., & Brunsden, D. (1996). Physico-chemical effects on the behaviour of a coastal mudslide. *Geotechnique*, *46*, 259–278.

Motellier, S., Ly, J., Gorgeon, L., Charles, Y., Hainos, D., Meier, P., & Page, J. (2003). Modelling of the ion-exchange properties and indirect determination of the interstitial water composition of an argillaceous rock. Application to the Callovo-Oxfordian low-water-content formation. *Applied Geochemistry*, *18*, 1517–1530.

Murphy, W. M., & Helgeson, H. C. (1989). Thermodynamic and kinetic constraints on reaction rates among minerals and aqueous solutions: IV. Retrieval of rate constants and activation parameters for the hydrolysis of pyroxene, wollastonite, olivine, andalusite, quartz and nepheline. *American Journal of Science*, *289*, 17–101.

Ng, C. W. W., & Shi, Q. (1998). A numerical investigation of the stability of unsaturated soil slopes subjected to transient seepage. Computer and Geotechnics 22. 1–28.

Novel, J.P., Dray, M., Fehri, A., Jusserand, C., Nicoud, G., Olive, P., Puig, J.M., Zuppi, G.M., (1999). Homogénéisation des signaux isotopiques 18O, 3H, dans un système hydrologique de haute montagne: la vallée d'Aoste (Italie). Revue des Sciences de l'Eau 12, 3-21.

Pairis, J. L. (1968). Nouvelles données sur le massif du Lan (Chapeau de Gendarme) au Sud de Barcelonnette (Basses-Alpes). Travaux du Laboratoire de Géologie de Grenoble. *Tome*, *44*, 323–328.

Palandri, J. L., Kharaka, Y. K., (2004). A compilation of rate parameters of water-mineral interaction kinetics for application to geochemical modeling. Menlo Park, Calif.: U.S. Dept. of the Interior, U.S. Geological Survey.

Parkhurst, D.L., & Appelo, C.A.J., (2013), Description of input and examples for PHREEQC version 3—A computer program for speciation, batch-reaction, one-dimensional transport, and inverse geochemical calculations: U.S. Geological Survey Techniques and Methods, book 6, chap. A43, 497 p., http://pubs.usgs.gov/tm/06/a43/.

Pearson, F. J., Tournassat, C., & Gaucher, E. C. (2011). Biogeochemical processes in a clay formation in situ experiment: Part E – Equilibrium controls on chemistry of pore water from the Opalinus Clay, Mont Terri Underground Research Laboratory, Switzerland. Applied Geochemistry, The in situ experiment on biogeochemical processes in the Opalinus Clay at the Mont Terri Underground Research Laboratory, Switzerland. *Applied Geochemistry*, *26*(6), 990–1008.

Picarelli, L., Urciuoli, G., Mandolini, A., & Ramondini, M. (2006). Softening and instability of natural slopes in highly fissured plastic clay shales. Natural Hazards and Earth System. *Science*, *6*, 529–539.

Roques, C., Bour, O., Aquilina, L., Dewandel, B., Leray, S., Schroetter, J. M., … Mougin, B. (2014). Hydrological behavior of a deep sub-vertical fault in crystalline basement and relationships with surrounding reservoirs. *Journal of Hydrology*, *509*, 42–54.

Saidi, D., Le Bissonnais, Y., Duval, O., Daoud, Y., & Halitim, A. (2004). Effet du sodium échangeable et de la concentration saline sur les propriétés physiques des sols de la plaine du Cheliff (Algérie). Etude et Gestion des Sols 11. 137–148.

Santamarina, J. C., Klein, K. A., Wang, Y. H., & Prencke, E. (2002). Specific surface: determination and relevance. *Canadian Geotechnical Journal*, *39*, 233–241.

Scislewski, A., & Zuddas, P. (2010). Estimation of reactive mineral surface area during water–rock interaction using fluid chemical data. *Geochimica et Cosmochimica Acta*, *74*, 6996–7007.

Seaton, W. J., & Burbey, T. J. (2005). Influence of ancient thrust faults on the hydrogeology of the Blue Ridge Province. *Ground Water*, *43*, 301–313.

Stumpf, A., Malet, J. P., Kerle, N., Niethammer, U., & Rothmund, S. (2012). Image-based mapping of surface fissures for the investigation of landslide dynamics. Geomorphology 186. 12–27.

Tacher, L., Bonnard, C., Laloui, L., & Parriaux, A. (2005). Modelling the behaviour of a large landslide with respect to hydrogeological and geomechanical parameter heterogeneity. *Landslides*, *2*, 3–14.

Toth, J. (1999). Groundwater as a geologic agent: An overview of the causes, processes, and manifestations. *Hydrogeology Journal*, *7*, 1–14.

Tournassat, C., Lerouge, C., Blanc, P., Brendlé, J., Greneche, J.-M., Touzelet, S., & Gaucher, E. C. (2008). Cation exchanged Fe(II) and Sr compared to other divalent cations (Ca, Mg) in the Bure Callovian–Oxfordian formation: Implications for porewater composition modelling. *Applied Geochemistry*, *23*, 641–654.

Travelletti, J., Sailhac, P., Malet, J. P., Grandjean, G., & Ponton, J. (2012). Hydrological response of weathered clay-shale slopes: water infiltration monitoring with time-lapse electrical resistivity tomography. *Hydrological Processes*, *26*, 2106–2119.

USGS, (2005). A Simple Field Leach Test to Assess Potential Leaching of Soluble Constituents from Mine Wastes, Soils, and Other Geologic Materials. USGS fast sheet 2500-3100.

Vallet, A., Bertrand, C., Mudry, J., Bogaard, T., Fabbri, O., Baudement, C., & Régent, B. (2015). Contribution of time-related environmental tracing combined with tracer tests for characterization of a groundwater conceptual model: A case study at the Séchilienne landslide, western Alps (France. *Hydrogeology Journal*, *23*, 1761–1779.

Van Asch, T. W. J., Buma, J., & Van Beek, L. P. H. (1999). A view on some hydrological triggering systems in landslides. *Geomorphology*, *30*, 25–32.

Williamson, M., & Rimstidt, J. (1994). The kinetics and electrochemical rate-determining step of aqueous pyrite oxidation. *Geochimica et Cosmochimica Acta*, *58*, 5443–5454.

Xu, T., Apps, J. A., Pruess, K., & Yamamoto, H. (2007). Numerical modeling of injection and mineral trapping of CO2 with H2S and SO2 in a sandstone formation. *Chemical Geology*, *242*, 319–346.

Zerai, B., Saylor, B. Z., & Matisoff, G. (2006). Computer simulation of CO2 trapped through mineral precipitation in the Rose Run Sandstone, Ohio. *Applied Geochemistry*, *21*, 223–240.

How to cite this article: V. Marc, C. Bertrand, J.-P. Malet, N. Carry, R. Simler, and F. Cervi (2016), Groundwater—Surface waters interactions at slope and catchment scales: Implications for landsliding in clay-rich slopes, *Hydrological Processes*, doi: 10.1002/hyp.11030